

Two different emissions of (2Z)-2-(4-bromophenyl)-3-[4-(dimethylamino)phenyl]prop-2-enitrile due to crystal habit and size: synthesis, optical and supramolecular characterization.

Judith Percino, Margarita Cerón, Perumal Venkatesan, Paulina Ceballos, Alejandro Bañuelos, Oscar Rodríguez, Maxime A. Siegler, Fernando Robles, Victor M. Chapela, Guillermo Soriano-Moro, Enrique Pérez-Gutiérrez, JOSE BONILLA-CRUZ, and Subbiah Thamotharan

Cryst. Growth Des., **Just Accepted Manuscript** • DOI: 10.1021/acs.cgd.6b01670 • Publication Date (Web): 21 Feb 2017

Downloaded from <http://pubs.acs.org> on February 24, 2017

Just Accepted

“Just Accepted” manuscripts have been peer-reviewed and accepted for publication. They are posted online prior to technical editing, formatting for publication and author proofing. The American Chemical Society provides “Just Accepted” as a free service to the research community to expedite the dissemination of scientific material as soon as possible after acceptance. “Just Accepted” manuscripts appear in full in PDF format accompanied by an HTML abstract. “Just Accepted” manuscripts have been fully peer reviewed, but should not be considered the official version of record. They are accessible to all readers and citable by the Digital Object Identifier (DOI®). “Just Accepted” is an optional service offered to authors. Therefore, the “Just Accepted” Web site may not include all articles that will be published in the journal. After a manuscript is technically edited and formatted, it will be removed from the “Just Accepted” Web site and published as an ASAP article. Note that technical editing may introduce minor changes to the manuscript text and/or graphics which could affect content, and all legal disclaimers and ethical guidelines that apply to the journal pertain. ACS cannot be held responsible for errors or consequences arising from the use of information contained in these “Just Accepted” manuscripts.



1
2
3
4
5
6
7 Two different emissions of (2Z)-2-(4-bromophenyl)-
8
9
10
11 3-[4-(dimethylamino)phenyl]prop-2-enitrile due to
12
13
14
15
16 crystal habit and size: synthesis, optical and
17
18
19
20 supramolecular characterization
21
22
23
24

25 *Judith Percino,^{1*} Margarita Cerón,¹ Perumal Venkatesan,¹ Paulina Ceballos,¹ Alejandro*
26 *Bañuelos,¹ Oscar Rodríguez,¹ Maxime A. Siegler,² Fernando Robles,¹ Víctor M. Chapela,¹*
27 *Guillermo Soriano-Moro,¹ Enrique Pérez-Gutiérrez,³ José Bonilla-Cruz⁴ and Subbiah*
28 *Thamotharan⁵*
29
30
31
32
33
34

35
36 ¹Lab. de Polímeros, Centro de Química, Instituto de Ciencias, Benemérita Universidad
37
38 Autónoma de Puebla, Complejo de Ciencias, ICUAP, Edif. 103H, 22 Sur y San Claudio, Puebla,
39
40 Puebla, México, C.P. 72570.
41
42

43
44 ²Department of Chemistry, Johns Hopkins University, New Chemistry Building, 3400 N.
45
46 Charles St. Baltimore, MD, 21218, USA.
47
48

49
50 ³CONACYT–Lab. de Polímeros, Centro de Química, Instituto de Ciencias, Benemérita
51
52 Universidad Autónoma de Puebla, Complejo de Ciencias, ICUAP, Edif. 103H, 22 Sur y San
53
54 Claudio, Puebla, Puebla, México, C.P. 72570.
55
56
57
58
59
60

1
2
3 ⁴Centro de Investigación en Materiales Avanzados S.C. (CIMAV-Unidad Monterrey), Av.
4
5 Alianza Norte 22, Autopista Monterrey-Aeropuerto Km 10, PIIT, Apodaca-Nuevo León,
6
7 México, C.P. 66600.
8
9

10
11 ⁵Biomolecular Crystallography Laboratory, Department of Bioinformatics, School of Chemical
12 and Biotechnology, SASTRA University, Thanjavur, 613 401, India.
13
14
15

16
17 **Corresponding author:**
18

19
20 Judith Percino;

21
22 judith.percino@correo.buap.mx;
23

24
25 Centro de Química, Instituto de Ciencias, Benemérita Universidad Autónoma de Puebla,
26
27 Complejo de Ciencias, ICUAP, Edif. 103H, 22 Sur y San Claudio, C.P. 72570, Puebla, Puebla.
28
29 México. Phone: +(52) 222 2295500 x7285.
30
31

32
33
34
35
36
37 ABSTRACT Optical and X-ray diffraction characterizations of crystals **I** and **II** of (2Z)-2-(4-
38 bromophenyl)-3-(4-(dimethylamino)phenyl)prop-2-enenitrile (Z-4-BrPhDMAPhACN) are
39 reported. **I** and **II** belong to the same monoclinic space group and have nearly identical unit-cell
40 dimensions [**I**: a = 11.0169(2); b = 6.02041(11); c = 21.8541(4); (β) 98.4082(18) and **II**: a =
41 11.0475(6); b = 6.0273(3); c = 21.8533(11); (β) 98.315(5)]. Crystals **I** and **II** were formed under
42 different conditions and have different crystal habits and colors: crystals **I** are yellow blocks,
43 whereas crystals **II** are small, orange needles. **I** and **II** show absorption maxima (λ_{abs}) in solution
44 at 404 nm and emission (λ_{em}) maxima at 501 nm (**I**) and at 502 nm (**II**). However, their emission
45 maxima are different in the solid state: **I** shows an emission at 512 nm and a shoulder at 534 nm,
46
47
48
49
50
51
52
53
54
55
56
57
58
59
60

1
2
3 whereas **II** exhibits a λ_{em} maximum at 582 nm. The differences in solid-state photoluminescence
4
5
6 were attributed to variations in the crystal morphology and to the crystal habit and size. Both **I**
7
8 and **II** were characterized by nuclear magnetic resonance, mass spectrometry, infrared
9
10 spectroscopy, UV-Vis spectroscopy, fluorescence, cyclic voltammetry, single-crystal and powder
11
12 X-ray diffraction, differential Scanning calorimetry, scanning electron microscopy and density
13
14 functional theory calculations.
15
16
17
18
19
20
21
22
23
24
25
26
27
28
29
30
31
32
33
34
35
36
37
38
39
40
41
42
43
44
45
46
47
48
49
50
51
52
53
54
55
56
57
58
59
60

1
2
3
4
5
6
7
8
9
10
11
12
13
14
15
16
17
18
19
20
21
22
23
24
25
26
27
28
29
30
31
32
33
34
35
36
37
38
39
40
41
42
43
44
45
46
47
48
49
50
51
52
53
54
55
56
57
58
59
60

Two different emissions of (2*Z*)-2-(4-bromophenyl)-3-[4-(dimethylamino)phenyl]prop-2-enenitrile due to crystal habit and size: synthesis, optical and supramolecular characterization

Judith Percino,^{1} Margarita Cerón,¹ Perumal Venkatesan,¹ Paulina Ceballos,¹ Alejandro Bañuelos,¹ Oscar Rodríguez,¹ Maxime A. Siegler,² Fernando Robles,¹ Víctor M. Chapela,¹ Guillermo Soriano-Moro,¹ Enrique Pérez-Gutierrez,³ José Bonilla-Cruz⁴ and Subbiah Thamocharan⁵*

¹Lab. de Polímeros, Centro de Química, Instituto de Ciencias, Benemérita Universidad Autónoma de Puebla, Complejo de Ciencias, ICUAP, Edif. 103H, 22 Sur y San Claudio, Puebla, Puebla, México, C.P. 72570.

²Department of Chemistry, Johns Hopkins University, New Chemistry Building, 3400 N. Charles St. Baltimore, MD, 21218, USA.

³CONACYT–Lab. de Polímeros, Centro de Química, Instituto de Ciencias, Benemérita Universidad Autónoma de Puebla, Complejo de Ciencias, ICUAP, Edif. 103H, 22 Sur y San Claudio, Puebla, Puebla, México, C.P. 72570.

⁴Centro de Investigación en Materiales Avanzados S.C. (CIMAV-Unidad Monterrey), Av. Alianza Norte 22, Autopista Monterrey-Aeropuerto Km 10, PIIT, Apodaca-Nuevo León, México, C.P. 66600.

⁵Biomolecular Crystallography Laboratory, Department of Bioinformatics, School of Chemical and Biotechnology, SASTRA University, Thanjavur, 613 401, India.

Corresponding author:

Judith Percino

Centro de Química, Instituto de Ciencias, Benemérita Universidad Autónoma de Puebla, Complejo de Ciencias, ICUAP, Edif. 103H, 22 Sur y San Claudio, C.P. 72570, Puebla, Puebla, México.

judith.percino@correo.buap.mx

ABSTRACT

Optical and X-ray diffraction characterizations of crystals **I** and **II** of (2Z)-2-(4-bromophenyl)-3-(4-(dimethylamino)phenyl)prop-2-enenitrile (Z-4-BrPhDMAPhACN) are reported. **I** and **II** belong to the same monoclinic space group and have nearly identical unit-cell dimensions [**I**: a = 11.0169(2); b = 6.02041(11); c = 21.8541(4); (β) 98.4082(18) and **II**: a = 11.0475(6); b = 6.0273(3); c = 21.8533(11); (β) 98.315(5)]. Crystals **I** and **II** were formed under different conditions and have different crystal habits and colors: crystals **I** are yellow blocks, whereas crystals **II** are small, orange needles. **I** and **II** show absorption maxima (λ_{abs}) in solution at 404 nm and emission (λ_{em}) maxima at 501 nm (**I**) and at 502 nm (**II**). However, their emission maxima are different in the solid state: **I** shows an emission at 512 nm and a shoulder at 534 nm,

1
2
3 whereas **II** exhibits a λ_{em} maximum at 582 nm. The differences in solid-state photoluminescence
4
5 were attributed to variations in the crystal morphology and to the crystal habit and size. Both **I**
6
7 and **II** were characterized by nuclear magnetic resonance, mass spectrometry, infrared
8
9 spectroscopy, UV-Vis spectroscopy, fluorescence, cyclic voltammetry, single-crystal and powder
10
11 X-ray diffraction, differential Scanning calorimetry (DSC), scanning electron microscopy (SEM)
12
13 and density functional theory calculations.
14
15
16
17
18
19
20
21
22

23 KEYWORDS: nanocrystals-emission, crystal habit, single-crystal X-ray diffraction, DSC, SEM,
24
25 bromophenylacetonitrile, PIXEL, Hirschfeld Surface.
26
27
28
29
30
31
32
33
34
35
36
37
38
39
40
41
42
43
44
45
46
47
48
49
50
51
52
53
54
55
56
57
58
59
60

INTRODUCTION

It is well known that different crystalline forms of the same substance can exhibit markedly different physical properties,¹⁻³ leading to a wide array of applications.⁴⁻⁶ Crystals or aggregates based on the same molecule are an active research topic in modern solid-state chemistry⁷ because the structure-property relations of materials could contribute to the design of new materials. For example, single-crystal X-ray diffraction and thermal analysis characterizations of 1,4-distyrylbenzene with different substituents showed a correlation between the substituents and structural properties due to the presence of two polymorphs obtained under different crystallization conditions.⁸ Differences in the photophysical properties of the two crystals were attributed to differences in the stacking modes of the chromophore and intermolecular electronic interactions in the crystals. Therefore, the effect of self-assembly and electronic interactions of molecules on the properties of a molecular solid is a fundamental and crucial aspect of material science. Recently, highly luminescent dicyanodistyrylbenzene crystals that exhibit an interesting mechanochromism have been reported.⁹ The behavior was explained by the presence of weak local dipole interactions, C–H \cdots π interactions, and C–H \cdots N hydrogen bonding in the molecular stacking assembly. The dicyanodistyrylbenzene polymorphs can be differentiated by the different modes of local dipole coupling, which cause a substantial alternation of the π – π overlap and excited state delocalization. These effects result in different colored fluorescence emissions and highly efficient deep/near-infrared emissions.¹⁰ In contrast, solid-state lighting (SSL) using organic chromophores has attracted much attention due to the potential applications of the latter in devices such as light-emitting diodes,¹¹⁻¹³ photovoltaic devices,¹⁴⁻¹⁶ and sensors.¹⁷⁻¹⁹ Tuning and controlling the emission wavelength of an organic material is crucial to identify the

1
2
3 appropriate application.^{20,21} The optical properties of different dyes in the solid state depend
4
5 strongly on the molecular structure and intermolecular interactions.²²⁻²⁴
6
7

8 Recently, organic chromophores that exhibit quenching of fluorescence in the solid state have
9
10 been reported, and this phenomenon is termed aggregation-caused quenching (ACQ). In contrast,
11
12 when the emission of fluorescence depends on the presence of the solid state, the process is
13
14 termed aggregation-induced emission (AIE) or aggregation-induced emission enhancement
15
16 (AIEE).²⁵⁻³¹ These organic materials may also exhibit no or weak fluorescence in solution,
17
18 whereas the aggregated particles (obtained by adding the solution into the poorly solubilizing
19
20 solvent) exhibit relatively intense fluorescence upon UV irradiation. Examples of such materials
21
22 are (dimethylamino)acrylonitrile derivatives, specifically Z-2-(phenyl)-3-(4-
23
24 dimethylaminophenyl)acrylonitrile³² and α -cyanostilbene.³³ A variety of AIE compounds have
25
26 been created and their fluorescence properties have been investigated.^{25-31,34-37} In most cases,
27
28 AIE is explained by the restriction of intramolecular rotation.³⁸
29
30
31
32
33

34 Herein, we report the synthesis, crystal structures, and optical characterization (absorption and
35
36 emission) of acrylonitrile containing the dimethylamine substituent as an electron donor, and
37
38 bromide and -CN as electron acceptors. The title compound, (2Z)-2-(4-bromophenyl)-3-[4-
39
40 (dimethylamino)phenyl]prop-2-enenitrile (Z-4-BrPhDMAPhACN), is completely characterized
41
42 using various techniques. The investigation reveals differences in the characteristic emission,
43
44 such as the enhancement of fluorescence in both a solvent and the solid state as well as the
45
46 photophysical properties. The data for the title compound are compared with those of the closely
47
48 related and analogous (2Z)-3-[4-(dimethylamino)phenyl]-2-phenylprop-2-enenitrile (**A**). Z-4-
49
50 BrPhDMAPhACN exhibits emission in solution and in the crystal form, depending on the habit
51
52 and size of the crystal. Additionally, Hirshfeld surfaces were calculated to analyze the
53
54
55
56
57
58
59
60

1
2
3 intermolecular interactions in a whole-molecule approach so the structure–property relationships
4
5 could be established unambiguously.
6
7

8 **EXPERIMENTAL SECTION**

9
10 **Single-crystal X-ray diffraction (SCXRD).** X-ray intensity data were collected for **I** and **II** at
11
12 110(2) K on a SuperNova diffractometer (equipped with an Atlas detector) with CuK α radiation
13
14 (mirror optics, $\lambda = 1.5418 \text{ \AA}$). The program CrysAlisPro (Version 1.171.36.24 Agilent
15
16 Technologies, 2012) was used to determine the unit cell dimensions. Analytical numerical
17
18 absorption correction based on a multifaceted crystal model was applied, using CrysAlisPro. The
19
20 temperature during data collection was controlled using a Cryojet system (manufactured by
21
22 Oxford Instruments). The crystal structures of **I** and **II** were solved by the SHELXS³⁹ program.
23
24 All non-hydrogen atoms were placed in idealized geometrical positions and constrained to ride
25
26 on their parent atoms, with $U_{\text{iso}}(\text{H}) = 1.2U_{\text{eq}}(\text{C})$. The methyl hydrogen atoms were also
27
28 constrained to an ideal geometry with $U_{\text{iso}}(\text{H}) = 1.5U_{\text{eq}}(\text{C})$ but were allowed to rotate about the N-
29
30 C bonds.
31
32
33
34
35

36 **Fourier transform infrared spectrometry (FT-IR).** The IR spectra of the products were
37
38 recorded from neat solids on a Vertex model 70 Bruker 750 FT-IR spectrophotometer with ATR
39
40 (Attenuated Total Reflection). The spectra were collected from 4000 to 400 cm^{-1} , with a 4 cm^{-1}
41
42 spectral resolution.
43
44

45 **Proton nuclear magnetic resonance (¹H-NMR).** Spectra were recorded using a Bruker 500-
46
47 MHz NMR spectrometer. The solvents CDCl₃, DMSO-d₆ and THF-d₈ were used.
48
49

50 **Mass spectrometry.** EI spectra were acquired using a Mass Spectrometer Jeol MStation 700-
51
52 D.
53
54
55
56
57
58
59
60

1
2
3 **Absorbance and emission (UV-Vis and PL).** Absorbance spectra were measured using a
4 SD2000 (Ocean Optics) spectrometer equipped with a pulse Xenon light source P-2 (Ocean
5 optics for the UV region (220-270 nm)), and a Cary 300 (Agilent) spectrometer equipped with a
6 deuterium and halogen lamp. For measurements (190-900 nm) in solution, the solvents used
7 were of spectroscopic grade and were subjected to preliminary checks to ensure the absence of
8 absorbing or fluorescent impurities within the scanned spectral ranges. For powder samples, the
9 absorption spectra were measured with KBr pellets using a DT 1000 CE light source (Analytical
10 Instrument Systems, Inc.). Emission spectra (PL) were acquired from a QE-Pro-FL (Ocean
11 Optics) equipped with a laser diode excitation source at a wavelength of 405 nm. The quantum
12 yields (Φ_f) of the three compounds (**I**, **II** and **A**) were determined as described by de Mello,⁴⁰
13 with slight modifications. In our fluorescence spectra measurements, the powdered samples
14 (prepared from crystals) were placed into quartz tubes instead of films. Alq₃ (Tris-(8-
15 hydroxyquinolinato)aluminium was used as reference in the quantum yield (Φ_f) measurements.
16
17
18
19
20
21
22
23
24
25
26
27
28
29
30
31
32
33

34 **Powder X-ray diffraction (PXRD).** Powder samples were characterized by powder X-ray
35 diffraction analysis using a Panalytical Empyrean diffractometer (Cu $K\alpha$ = 1.54178 Å). The
36 samples were scanned over the 2θ range of 5 to 100°.
37
38
39
40

41 **Scanning Electron Microscopy (SEM).** The morphology of the crystals was examined using
42 a scanning electron microscope (Nova NanoSEM 200, FEI) operating at 5 kV. The samples were
43 mounted on a slide glass under vacuum in an argon atmosphere prior to observation.
44
45
46
47

48 **Differential Scanning Calorimetry (DSC).** DSC thermograms of the samples (1-2 mg) were
49 recorded by a thermal analysis system (TA Instruments DSC Q200). The measurements were
50 performed in aluminum-pierced lid pans (Tzero) at a heating rate of 10 °C/min under a nitrogen
51
52
53
54
55
56
57
58
59
60

1
2
3 atmosphere (100 mL/min) over the range of 25–195 °C. The samples were cooled at the same
4
5 rate of 10 °C/min from 195 °C to 25 °C.
6
7

8 **Films deposition.** Organic films were deposited onto glass substrates. The substrates were
9
10 cleaned and treated with oxygen plasma for 5 min before deposition. Then, they were transferred
11
12 to an evaporation chamber, and 10 mg of the fluorescent compound was evaporated onto the
13
14 substrates at a ratio of 0.5 Å/s under a pressure of 10^{-6} Torr. The samples were monitored by a
15
16 Keyence VHX-5000 optical microscope with 500X magnification. The fluorescence
17
18 measurements were conducted using a Mineral Light UV-Lamp with an excitation at 350 nm and
19
20 a detector consisting of an Ocean Optics spectrometer coupled to an optic fiber.
21
22
23

24 **Cyclic Voltammetry (CV).** Measurements were carried out with a potentiostat
25
26 (PGSTAT128N), using a three-electrode cell assembly comprising Ag/Ag⁺ in a 3 M solution of
27
28 KCl as a reference electrode, a platinum wire ($\phi=0.2$ mm) as the working electrode, a 0.1 M
29
30 solution of tetrabutylammonium hexafluorophosphate (TBAFP₆) CH₂Cl₂ as a supporting
31
32 electrolyte and a platinum wire as the counter electrode. Ferrocene was used as an external
33
34 standard. The scanning rate was 50 mV/s.
35
36
37

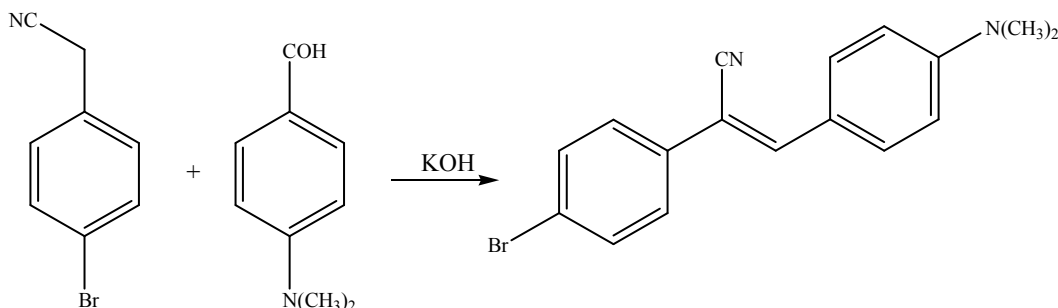
38 **Computational details.** Density functional theory (DFT) calculations were performed using
39
40 the Gaussian 09 program package.⁴¹ The crystal structure of each respective compound was
41
42 taken as the initial model for gas-phase geometric optimization at the M06-2X/cc-pVTZ level of
43
44 theory. The vibrational frequencies were calculated at the same level of theory to assess the
45
46 stationary point. No negative frequency was observed for the optimized models. For the optical
47
48 part, calculations of properties were performed by time-dependent DFT (TDDFT) with the time-
49
50 dependent Kohn-Sham formalism.⁴²
51
52
53
54
55
56
57
58
59
60

1
2
3 **Hirshfeld surface (HS) analysis and PIXEL energy calculation.** The Hirshfeld surface and
4 two-dimensional fingerprint (FP) plots were generated using Crystal Explorer 3.1,⁴³ as described
5 previously.⁴⁴ The lattice energies and intermolecular interaction energies were evaluated using
6 the PIXEL method. The distances involving hydrogen atoms were moved to their neutron values
7 before the calculation.^{43,44} The electron density of the molecule was obtained at the MP2/6-
8 31G** level of theory using the Gaussian 09 program.

17 SYNTHESIS AND CRYSTALLIZATION

19 **Chemicals.** 4-Bromophenylacetonitrile, 4-(dimethylamino)benzaldehyde, *N*-methylamino-
20 ethanol and CuI were purchased from Aldrich Chemical Co. (Mexico). KOH and K₂CO₃ were
21 purchased from J.T. Baker. DMSO and ethanol were acquired from Fermont. The reagents and
22 solvents were used as received.

23 **Synthesis of (2*Z*)-2-(4-bromophenyl)-3-(4-[dimethylamino]phenyl)prop-2-enitrile [(*Z*-
24 4-BrPhDMAPhACN)].** *Z*-4-BrPhDMAPhACN was synthesized as shown in Scheme 1. Briefly,
25 a solution of 4-(dimethylamino)benzaldehyde (1.0 equiv.) in 10 mL of ethanol, 4-
26 bromophenylacetonitrile (1.0 equiv.) and KOH (4.0 equiv.) was stirred at room temperature for
27 12 h. Upon completion of the reaction, a dark yellow precipitate was obtained, which was
28 washed with ethanol at 4 °C. The final product was recrystallized from a cyclohexane: ethyl
29 acetate mixture (1:2 v/v). The m.p. and yield of the product were found to be 192-194 °C and
30 85%, respectively.



1
2
3 **Scheme 1.** Reaction to obtain (2Z)-2-(4-bromophenyl)-3-(4-[dimethylamino]phenyl)prop-2-
4 enenitrile (Z-4-BrPhDMAPhACN)
5
6

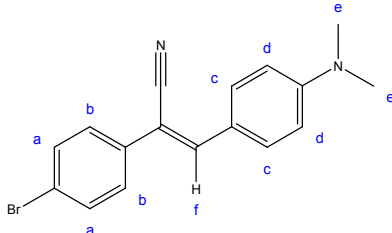
7
8 **Preparation of crystals I, I*, I** and II.** Single crystals of **I** were obtained from cyclohexane
9 by slow evaporation. Briefly, 0.020 g of the title compound was dissolved in 25 mL of
10 cyclohexane, heated at 75 °C for 5 min and allowed to evaporate at room temperature (25 °C).
11 Crystals appeared after 18 h and were allowed to grow for another 12 h. The crystals were
12 filtered, washed with cyclohexane and used for further studies. The melting point of crystal **I** was
13 found to be 190-192 °C. We tried to replace the bromine atom in the title compound by an *N*-
14 methylaminoethanol group using the Ullmann coupling reaction. Unexpectedly, crystals of **II**
15 were identified. The experimental procedure is briefly summarized in the supplementary
16 information section (S1). Crystals **II** were obtained from two different solvents (DMSO and
17 DMF) without any other supporting reagents. Briefly, 0.02 g of the title compound was dissolved
18 in 25 mL of DMSO or DMF, heated at 110 °C for 4 h and allowed to evaporate slowly at room
19 temperature. The title compound also crystallized from DMF (**I***) and DMSO (**I****) solvents at
20 100 °C.
21
22
23
24
25
26
27
28
29
30
31
32
33
34
35
36
37
38

39 **RESULTS AND DISCUSSION**

40
41 The title compound, Z-4-BrPhDMAPhACN acrylonitrile, was synthesized as shown in
42 Scheme 1. Similar compounds have been synthesized using piperidine as a catalyst, as reported
43 earlier by our laboratory. Here, we used KOH as a catalyst for improving the reaction conditions
44 and yield. The synthesized compound was characterized by IR, ¹H-NMR, EI mass spectrometry
45 and single-crystal X-ray diffraction studies. The title compound Z-4-BrPhDMAPhACN is
46 compared with an analogous compound **A**.³² Compound **A** exhibits weak fluorescence in
47 solution but also displays the AIE property.³² For the title compound, crystals (**I**, **I***, **I**** and **II**)
48
49
50
51
52
53
54
55
56
57
58
59
60

were obtained from different conditions. These crystals were extensively characterized by ^1H -NMR, using different deuterated solvents (such as CDCl_3 , DMSO-d_6 , and THF-d_8). The details of chemical shifts for **I**, **I***, **I**** and **II** are presented in Table 1.

Table 1. Chemical shifts (in ppm) of **I**, **II**, **I***, and **I**** in different solvents and EI mass spectrometry

						EI (I/%), m/z
Chemical shifts δ (ppm) and coupling constants J (Hz)						
I CDCl_3	7.88–7.86 (d, 2Ha, J = 10.0 Hz)	7.55–7.50 (m, 4Hb,c, J = 10.0 Hz)	7.40 (s, 1Hf)	6.74–6.72 (d, 2Hd, J = 10.0 Hz)	3.09 (s, 6He)	327(64) [M+], 326(100) base peak, 329(27) [M+2], 325(45), 203(19), 123(9), 18(25)
I THF	7.94–7.92 (d, 2Ha, J = 10 Hz)	7.65–7.59 (m, 5Hb,c,f, J = 10.0 Hz)		6.83–6.81 (d, 2Hd, J = 10.0 Hz)	3.09 (s, 6He)	
I* THF	7.94–7.92 (d, 2Ha, J = 10.0 Hz)	7.65–7.59 (m, 5Hb,c,f, J = 5.0, 10.0 Hz)		6.83–6.81 (d, 2Hd, J = 10.0 Hz)	3.09 (s, 6He)	
I DMSO-d_6	7.87–7.86 (d, 2Ha, J = 5.0 Hz)	7.68–7.62 (m, 4Hb,c, J = 5.0, 10.0 Hz)	7.89 (s, 1Hf)	6.83–6.81 (d, 2Hd, J = 10.0 Hz)	3.39 (s, 6He)	
I** CDCl_3	7.88–7.86 (d, 2Ha, J = 5.0, 10.0)	7.56–7.50 (m, 4Hb,c, J = 10.0 Hz)	7.40 (s, 1Hf)	6.75–6.73 (d, 2Hd, J = 10.0 Hz)	3.09 (s, 6He)	

	(Hz)					
I** DMSO- d ₆	7.87–7.86 (d, 2Ha, J = 5.0 Hz)	7.67–7.62 (m, 4Hb,c, J = 5.0, 10.0 Hz)	7.89 (s, 1Hf)	6.83–6.61 (d, 2Hd, J = 10.0 Hz)	3.03 (s, 6He)	
II CDCl ₃	7.89–7.87 (d, 2Ha, J = 10.0 Hz)	7.56–7.51(m, 4Hb,c, J = 5.0, 10.0 Hz)	7.41 (s, 1Hf)	6.76–6.74 (d, 2Hd, J = 5.0, 10.0 Hz)	3.10 (s, 6He)	327(64) [M+], 326(100) base peak, 329(27) [M+2], 325(44), 203(18), 123(9), 115(4), 18(26)
II DMSO- d ₆	7.89–7.77 (m, 3Ha, J = 5.0 Hz)	7.67–7.62 (m, 4Hb,c, J = 5.0, 10.0 Hz)		6.83–6.81 (d, 2Hd, J = 10.0 Hz)	3.37 (s, 6He)	
II THF	7.94–7.92, (d, 2Ha, J = 10.0 Hz)	7.65–7.59 (m, 5Hb,c,f, J = 10.0 Hz)		6.82–6.81 (d, 2Hd, J = 10.0 Hz)	3.09 (s, 6He)	

* = **I** treated with DMF for at 100°C, 24h (orange crystals); ** = **I** treated with DMSO at 100°C, 24h (yellow-orange crystals)

The signals in the ¹H-NMR spectra of **I** and **II** are presented in Table 1. The chemical shift of the proton assigned to -CHf=CNC- appears as a singlet at 7.40 ppm for both **I** and **II** in CDCl₃. The signals at 7.88–7.86 ppm correspond to 2Ha; the signals at 7.55–7.50 ppm are assigned to Hb,c, which shows an integration corresponding to four protons; the signals at 6.74–6.72 ppm correspond to 2Hd; and the methyl groups (He) appear at 3.09 ppm. Additionally, the results of the fragmentation patterns (see S1) give the following ion abundance (I/%) vs m/z, for **I**: 327(64) [M+], 326(100) base peak, 329 (27) [M+2], 325(45), 203(19), 123(9), 18(25), for **II**: 327(64) [M+], 326(100) base peak, 329(27) [M+2], 325(44), 203(18), 123(9), 115(4), 18(26), Table 1.

Crystals of **I** and **II** are acquired in polar and nonpolar aprotic solvents.⁴⁵ The chemical shift of the proton Hf is at 7.89 ppm in DMSO-d₆, and it overlaps with the two protons assigned as Hb and Hc yielding a multiplet at 7.67–7.62 ppm in THF-d₈. The protons Ha, Hb and Hc display shifts from 7–8 ppm to a low field, whereas the chemical shift of methyl groups does not undergo a strong change. Intramolecular hydrogen bonds affect the proton Hf by their

1
2
3 environment, shifting it downfield. Intramolecular hydrogen bonds do not have such an effect.
4
5 Therefore, monitoring the structural changes of *Z*-4-BrPhDMAPhACN and **A** by ¹H-NMR at
6
7 room temperature reveals the presence of small signals that may indicate *E*-*Z* isomerization.⁴⁶⁻⁴⁸
8
9

10 For **A**, the signal from the H proton of the acrylonitrile -CNC=CH- is found to be overlapped
11 with the signals from the protons in the *ortho* position on the aromatic ring attached to -CCN=.
12
13 However, in DMSO-d₆ and THF, the proton chemical shifts are appreciable, but the protons on
14
15 the double bond move to the deshielding zone, appearing at 7.82 ppm in DMSO-d₆ and as a
16
17 singlet signal at 7.61 ppm in THF. This behavior is important because it could give an indication
18
19 of the change in dipole moment (μ) upon photoluminescence and quenching in solution
20
21 conditions.⁴⁹
22
23
24
25
26

27 The Fourier transform infrared (FT-IR) spectrum shows important signals at 2205 cm⁻¹ due to
28 the -CN group, displaying a strong conjugation at 1611 cm⁻¹ due to the double bond and at 1580
29
30 cm⁻¹ due to the ν C=C assigned to the conjugated aryl group. The δ C-H for the tri-substituted
31
32 double bond is observed at 810 cm⁻¹ for **A**. The IR spectra show only small differences between
33
34 the crystals; the absorption band occurring at 816 cm⁻¹ in **I** and 818 cm⁻¹ in **II** is assigned to δ C-
35
36 H of the trisubstituted double bond -C=CCN. This value indicates an effect of the Br atom in the
37
38 *para* position. The corresponding peak is slightly shifted in **I** and **II** compared to **A** (at 810 cm⁻¹).
39
40 The intensity of the peak at 2360 cm⁻¹ in **I** is decreased as compared to **II**. For the functional
41
42 group ν C \equiv N attached to the alkene double bond, a peak is observed at 2205 cm⁻¹ for both
43
44 crystals **I** and **II**. This signal has a strong intensity, sharp absorption, and a lower frequency than
45
46 those attributed to conjugation with double bonds.⁵⁰ The δ_{as} and δ_s bands for -CH₃ are observed
47
48 at 1443 and 1375 cm⁻¹, respectively. For the aromatic rings, the ν C=C absorptions occur at 1580
49
50 and 815 cm⁻¹, in accordance with the reported values.⁵⁰ The typical overtone/combination bands
51
52
53
54
55
56
57
58
59
60

1
2
3 appear at 1994 cm⁻¹ and 1806 cm⁻¹ and indicate the expected ring substitution patterns in **I** and
4
5 **II**. In the region of 1335–1250 cm⁻¹, no variations are observed for **I** and **II** (see S1). The IR
6
7 spectra of **A** and crystals **I** and **II** show variations in the intensity of bands in the range ~550-850
8
9 cm⁻¹. Vibrations due to the motions of C_{Ar}-H of the ring are more intense in **A**, whereas in **I** and
10
11 **II**, similar bands are not seen or are weak in intensity. This may indicate the presence of bromine
12
13 on the aromatic ring. In contrast, the C-Br stretch of the *p*-bromophenyl- moiety cannot be
14
15 assigned clearly because C-H fingerprints appear in this range. Additionally, the intensities of
16
17 δC-H in both aromatic rings are changed. This finding suggests that these vibrations are more
18
19 intense when Br is attached on the phenyl group. νC-C is assigned at 1067 cm⁻¹ for **A** and at
20
21 1072 cm⁻¹ for **I** and **II**, being shifted to a higher frequency and giving stronger signals for **I** and
22
23 **II**.

24
25
26
27
28
29 **Single-crystal X-ray Crystallography.** Structural determination by single-crystal X-ray
30
31 diffraction reveals that both crystals are ordered and identical (*i.e.*, characterized by the same
32
33 unit-cell parameters, Z number, crystal system, and space group). The main difference is that the
34
35 title compound crystallizes in two different crystal habits (**I**: yellow blocks and **II**: orange
36
37 needles, Figure 1). The crystal data and structure refinement details for crystals of **I** and **II** are
38
39 summarized in Table 2. The molecular structure of compound **A**³² is comparable to those of **I**
40
41 and **II**, although the phenyl group formed by the C(12)-C(17)-C(13)-C(14)-C(15)-C(16) atoms is
42
43 substituted with a bromine atom. The electronic density is distributed almost homogeneously over
44
45 the whole ring. The C(12)-C(17) bond lengths in **I** and **II** are elongated (1.401 Å and 1.413 Å for
46
47 **II**) compared with **A**. This elongation possibly indicates that the distribution of charge density is
48
49 located *anti* to the electron-withdrawing –CN for all structures and that the overall values are
50
51 slightly different from the standard value of 1.380 Å for *Car*=*Car* in a phenyl ring.⁵¹ The C(10)-
52
53
54
55
56
57
58
59
60

C(12) bond length values (Csp^2-Car) for a conjugated double bond in **(I)**, **(II)**, and **(A)** are slightly larger than the typical value (1.470 Å). This could be an effect of the strongly electron-withdrawing $-CN$ group. In general, the degree of π -electron delocalization is identical in **I** and **II** due to the identical values within standard uncertainties⁵¹ (see Table 3 and S1). As shown in Figure 2, the structures **I**, **II** and **A** superimpose well, and the maximum root mean square deviation (rmsd: 0.095 Å) is observed for **II** and **A**. It is worth noting that the overall conformations and crystal packing of **I** and **II** are nearly identical. Therefore, the changes in fluorescence emission observed in **I** and **II** are not an effect of the crystal packing. It is of interest to mention that the C(2)-N(1) bond length in **II** is significantly shorter than that in **I**.

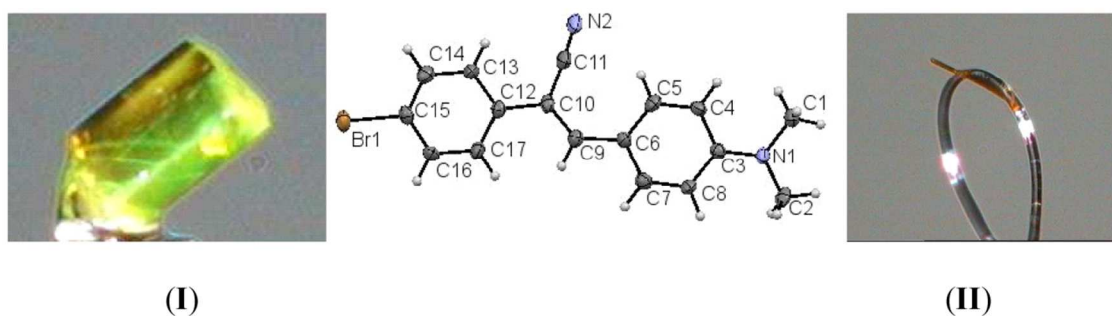


Figure 1. Crystal habits of **I** and **II** and ORTEP diagram of (2*Z*)-2-(4-bromophenyl)-3-[4-(dimethylamino)phenyl]prop-2-enitrile, showing the displacement ellipsoids drawn at a 50% probability level.

Table 2. Crystal data and refinement parameters for (2*Z*)-2-(4-bromophenyl)-3-[4-(dimethylamino)phenyl]-prop-2-enitrile

	I	II
Empirical formula	C ₁₇ H ₁₅ Br N ₂	C ₁₇ H ₁₅ Br N ₂
Crystal system	Monoclinic	Monoclinic
Color, Habit	Yellow, block	orange, needle
Formula weight	327.22	327.22
Space group	P 2 ₁ /c	P 2 ₁ /c
T(K)	110(2)	110(2)

a(Å)	11.0169(2)	11.0475(6)
b(Å)	6.02041(11)	6.0273(3)
c(Å)	21.8541(4)	21.8533(11)
γ (°);	98.4082(18)	98.315(5)
V(Å ³)	1433.92(5)	1439.84(13)
Z	4	4
Dc(g cm ⁻³)	1.516	1.510
F(000)	664	664
μ (mm ⁻¹)	3.817	3.802
λ (Å)	1.54178	1.54178
Crystal size (mm ³)	0.30 × 0.23 × 0.21	0.25 × 0.18 × 0.09
2 θ max(°)	143.8	143.8
N	9545	10017
Nunique, N(I>2.0 σ (I))	2809, 2652	3497 (including the overlapped reflections from the second twin component), 1947
R ₁	2.20	4.51
wR ₂	5.66	9.34
goodness-of-fit	1.051	0.776
Largest diff peak and hole (e Å ⁻³)	0.29 and -0.36	0.89 and -0.45

Table 3. Selected bond lengths (Å) and torsion angles (°) in **I** and **II** of (2Z)-2-(4-bromophenyl)-3-[4-(dimethylamino)phenyl]prop-2-enenitrile

Bond lengths	I	II	A
C(1)-N(1)	1.448(2)	1.443(6)	1.447(3)
C(2)-N(1)	1.4500(19)	1.409(6)	1.454(3)
C(3)-N(1)	1.366(2)	1.369(5)	1.371(3)
C(6)-C(9)	1.447(2)	1.462(5)	1.454(3)
C(10)-C(11)	1.439(2)	1.436(7)	1.441(3)
C(10)-C(12)	1.484(2)	1.491(6)	1.496(3)
C(12)-C(17)	1.401(2)	1.413(6)	1.393(3)
C(11)-N(2)	1.149(2)	1.145(7)	1.151(3)
C(15)-Br(1)	1.8961(15)	1.904(4)	
Torsion angle (°)			
C(8)-C(3)-N(1)-C(1)	-176.94(14)	-176.7(5)	-6.0(3)
C(4)-C(3)-N(1)-C(1)	2.7(2)	2.5(8)	174.6(2)
C(8)-C(3)-N(1)-C(2)	-5.8(2)	-5.2(8)	-170.1(2)
C(4)-C(3)-N(1)-C(2)	173.89(14)	174.0(5)	10.5(3)

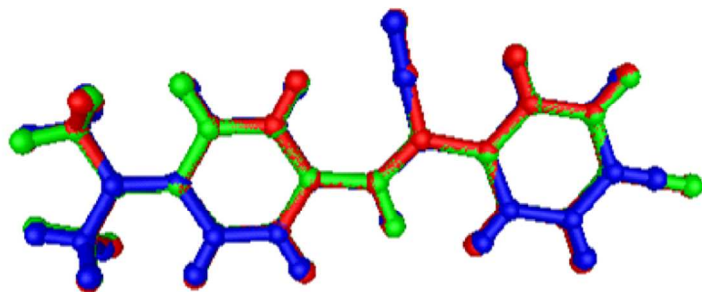
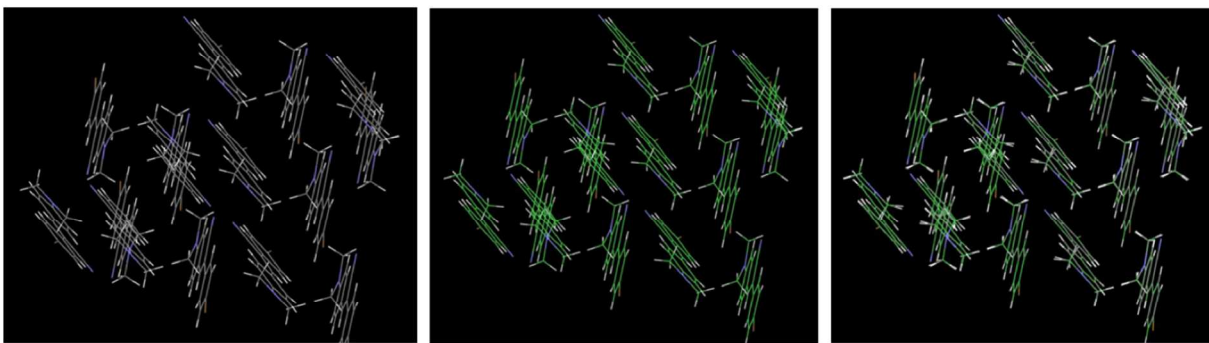


Figure 2. Structural superimposition of **I** (red), **II** (green), and **A** (blue).

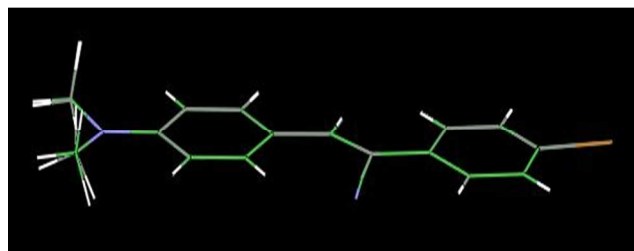
Structural overlay studies were carried out to identify the conformational changes in the structures of crystal **I**, **II** and their parent compound (**A**). Common atoms other than the *N,N*-dimethyl group and Br atom were used for the structural superposition. The root mean square deviation (rmsd) between **I** and **II** is 0.011 Å. The rmsd between **I** and **A** is 0.094 Å, and that between **II** and **A** is 0.095 Å. It is worth noting that the structures **I**, **II** and their parent structure (**A**) are well superimposable, apart from the difference observed in the hydrogen atoms of the *N,N*-dimethyl group (Figure 2). No other significant difference is observed in the structures of **I**, **II** and **A**.

Usually, the arrangement of the molecular structure in a crystal is influenced by the intermolecular strain experienced by each molecule.⁵² A molecular structure can experience three different types of strain: angular strain, torsional strain and steric strain. Due to the interactions and repulsions between different molecules in the packing, the contact distances between molecules can be affected by any, all, or none of these three strains. In the present report, the torsion angles of **I** and **II** are identical within the standard uncertainties (Table 3 and S1), indicating that the crystal packing of **I** and **II** is the same. Therefore, the differences between the fluorescence emission spectra of **I** and **II** are not related to crystal packing, as described in other reports, Figure 3(a). In contrast, it can be seen that the C(2)-N(1) bond length of **II** is

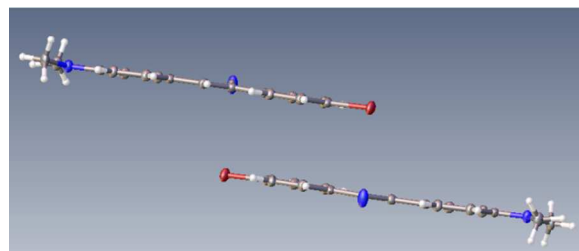
1
2
3 significantly shorter than that of **I** owing to $-\text{CH}_3$. This is an indication of the light twist present
4
5 in the $(\text{CH}_3)_2\text{N}$ - moiety, Figure 3(b). When a part of a molecule is able to rotate around a sigma
6
7 bond, different levels of torsional strain are generated and vary with the placements of the
8
9 bond, different levels of torsional strain are generated and vary with the placements of the
10
11 substituents relative to each other. This leads to different conformations of molecules, which
12
13 affect the π - π interactions in the solid and thus affect the optical properties. Figure 3(b) depicts
14
15 the overlap of both molecular structures **I** and **II**. The torsion angles for the molecules in **I** and **II**
16
17 remain unchanged, and consequently, there is no change in the molecular conformation. The
18
19 intermolecular potentials UNI (Unified pair-potential parameters), attributed to molecular forces,
20
21 were calculated using the Mercury program⁵³ as an approach toward the total lattice energies.⁵⁴⁻⁵⁷
22
23 The value of -146.20 kJ/mol was obtained for **A**, 161.04 kJ/mol for **I**, and 161.39 kJ/mol for **II**.
24
25 Additionally, values of the strongest interactions were obtained by calculating the packing
26
27 energy from intermolecular potentials.
28
29
30
31



(a)



(b)



(c)

1
2
3 **Figure 3.** Crystal packing diagrams of **I** (gray) and **II** (green) and overlap of both (gray-green)⁵³
4
5 (a) molecular structure overlap of **I** and **II** (b), and perspective view of the structures showing the
6
7 strong $\pi\cdots\pi$ interactions (c).⁵⁸
8
9

10
11 The packings of **I** and **II** are illustrated in Figure 3(a), which shows a typical herringbone
12 arrangement. The crystal packing is identical for both structures. The herringbone packing mode
13 features a co-facial π -stacking motif that is important for favorable electronic transfer properties,
14 with the principal difference being that of molecule **A**. As illustrated in Figure 3(c), the
15 molecules in **I** and **II** show a tilted face-to-face arrangement for the *p*-bromophenyl, with a
16 centroid-centroid distance of 3.710 Å and a shift distance of 1.244 Å for **I** and with
17 corresponding values of 3.722 Å and 1.256 Å for **II** (these distances were calculated using
18 OLEX 2⁵⁸). These are typical values of aromatic $\pi\cdots\pi$ interaction centroid distances (*i.e.* > 3.65 Å
19 and offsets of 1-6-1-8 Å).⁵⁹
20
21
22
23
24
25
26
27
28
29
30
31

32
33 **PIXEL Calculation and Hirshfeld surface (HS) analysis.** *PIXEL analysis.* The overall
34 lattice energies for **I**, **II** and **A** crystals and the intermolecular interaction energies for various
35 pairs extracted from respective crystal structures have been evaluated using the PIXEL
36 method.⁶⁰⁻⁶² The overall lattice energies for these three crystals are presented in Table 4. The
37 lattice energy is nearly the same for both **I** and **II**. It is worth noting that crystal **A** is ~2 kcal mol⁻¹
38 less stable than are crystals **I** and **II**. The intermolecular interaction energies for different pairs
39 in **I**, **II** and **A** are listed in Table 5. This result clearly shows that the intermolecular C-H $\cdots\pi$ and
40 $\pi\cdots\pi$ interactions are contribute significantly to the crystal packing. As shown in Figure 4,
41 dimer-I is formed by intermolecular C-H $\cdots\pi$ and $\pi\cdots\pi$ interactions in **I** and **II**. The interaction
42 energy for this dimer is -10.8 kcal mol⁻¹. The second most significant contribution to the crystal
43 packing of **I** and **II** comes from the combination of intermolecular C-H \cdots N and C-H $\cdots\pi$
44
45
46
47
48
49
50
51
52
53
54
55
56
57
58
59
60

interactions. The interaction energy for this dimer is $-8.5 \text{ kcal mol}^{-1}$. The methyl groups of the dimethylamino moiety participate in intermolecular C–H \cdots N and C–H \cdots π interactions. Dimer-III is stabilized by the methyl \cdots methyl (C1–H1C \cdots C2–H2C) interaction, whose interaction energy is calculated to be $-5.0 \text{ kcal mol}^{-1}$. Dimer-IV is formed by $\pi\cdots\pi$ stacking interaction, and it is found to have the same energetic strength as that of Dimer-III. The least contributing motif (dimer-V) in **I** and **II** is formed by an intermolecular C–H \cdots N interaction.

Table 4. Lattice energies (kcal mol^{-1}) partitioned into Coulombic, polarization, dispersion and repulsion terms for **I**, **II** and **A**

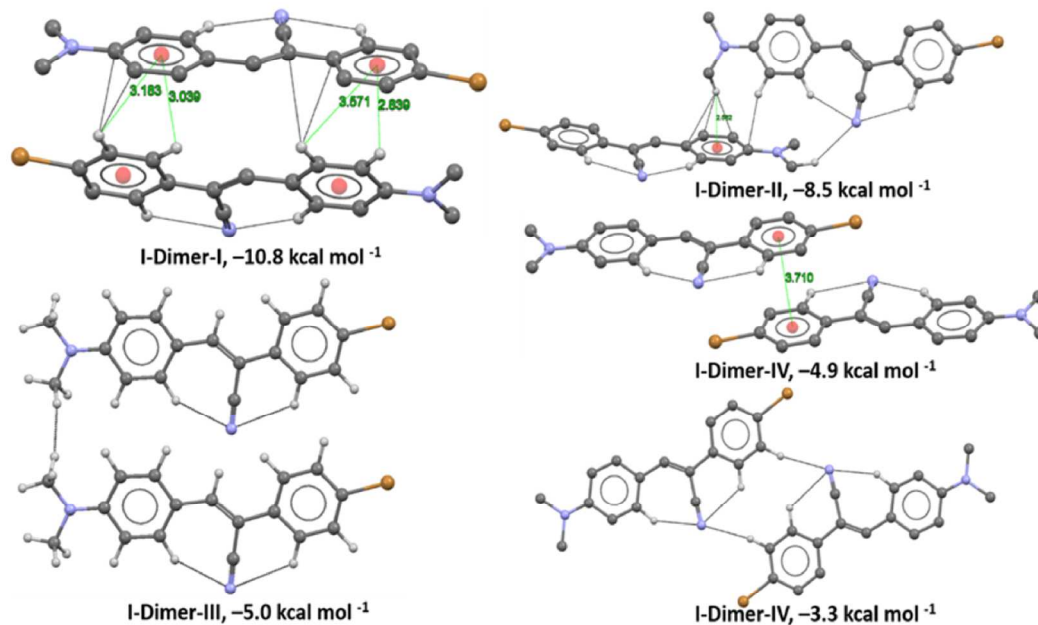
<i>Crystal</i>	E_{coul}	E_{pol}	E_{Disp}	E_{rep}	E_{tot}
I	-4.35	-5.14	-41.42	14.75	-36.14
II	-4.42	-5.09	-40.73	13.65	-36.59
A	-3.27	-5.80	-36.11	11.78	-34.54

Table 5. Interaction energies (E_{Tot}) partitioned into Coulombic (E_{Coul}), polarization (E_{Pol}), dispersion (E_{Disp}) and repulsion (E_{rep}) contributions (in kcal mol^{-1}) for various molecular pairs in **I**, **II** and **A**

<i>Dimer</i>	<i>Distance^a</i>	E_{coul}	E_{pol}	E_{Disp}	E_{rep}	E_{tot}	Symmetry	Important interactions	Geometry(\AA , $^\circ$)			HS Label
									H \cdots A	D \cdots A	D–H \cdots A	
Crystal I												
1	5.318	-3.8	-1.8	-15.0	9.8	-10.8	$-x, 1/2+y, 1/2-z$	C8–H8 \cdots Cg2	2.839	3.635	130.4	
								C7–H7 \cdots Cg2	3.571	3.991	105.0	
								C17–H17 \cdots Cg1	3.039	3.669	117.6	
								C16–H16 \cdots Cg1	3.183	3.731	112.3	
								C7–H7 \cdots C10	2.839	3.618	128.8	
								C7–H7 \cdots C12	2.897	3.535	117.9	
								C16–H16 \cdots C3	2.651	3.415	127.1	1
2	11.936	-4.7	-1.6	-8.7	6.5	-8.5	$1-x, -1/2+y, 1/2-z$	C16–H16 \cdots C8	2.894	3.754	136.4	
								C1–H1A \cdots Cg1	2.562	3.554	152.0	2
								C1–H1B \cdots N2	2.657	3.587	143.6	
								C1–H1A \cdots C6	2.840	3.610	128.1	
								C1–H1A \cdots C7	2.696	3.663	148.5	
								C1–H1A \cdots C8	2.800	3.881	175.6	
3	6.020	-0.6	-1.4	-7.5	4.4	-5.0	$x, -1+y, z$	C4–H4 \cdots C3	2.829	3.704	137.8	
								C1–H1C \cdots H2C–C2	2.048	2.987	156.7	3

4	6.760	-0.9	-0.6	-9.6	6.1	-4.9	$-x, 2-y, 1-z$	Cg2...Cg2		3.710		
5	8.540	-0.9	-1.3	-4.6	3.6	-3.3	$-x, 1-y, 1-z$	C14-H14...N2	2.531	3.653	159.0	4
Crystal II												
1	5.329	-3.7	-1.8	-14.8	9.5	-10.8	$-x, 1/2+y, 1/2-z$	C8-H8...Cg2	2.844	3.642	130.6	
								C7-H7...Cg2	3.570	3.995	105.3	
								C17-H17...Cg1	3.037	3.677	118.4	
								C16-H16...Cg1	3.204	3.753	112.4	
								C16-H16...C3	2.667	3.437	127.6	1
								C7-H7...C10	2.832	3.622	129.8	
2	11.962	-4.6	-1.6	-8.6	6.3	-8.6	$1-x, -1/2+y, 1/2-z$	C7-H7...C12	2.894	3.544	118.7	
								C1-H1A...Cg1	2.588	3.565	149.7	
								C1-H1B...N2	2.574	3.604	158.6	5
								C1-H1A...C7	2.827	3.682	135.8	
3	6.027	-0.5	-1.2	-7.1	3.7	-5.1	$x, -1+y, z$	C1-H1A...C8	2.844	3.883	160.9	
								C4-H4...C3	2.816	3.702	139.0	
4	6.750	-0.8	-0.6	-9.5	5.9	-5.0	$-x, 2-y, 1-z$	C1-H1C...H2C-C2	2.153	3.031	136.4	3
5	8.535	-0.9	-1.3	-4.6	3.5	-3.3	$-x, 1-y, 1-z$	Cg2...Cg2		3.722		
5	8.535	-0.9	-1.3	-4.6	3.5	-3.3	$-x, 1-y, 1-z$	C14-H14...N2	2.531	3.567	159.6	4
Compound A												
1	8.320	-4.5	-1.4	-8.1	5.4	-8.6	$-x, -y, 1/2+z$	C2-H2A...Cg1	2.604	3.638	159.3	
								C1-H1C...Cg1	3.723	4.650	144.8	
								C2-H2A...C6	2.811	3.594	129.1	
								C2-H2A...C7	2.782	3.692	135.0	
2	4.805	-2.5	-1.6	-12.7	8.8	-8.0	$1-x, -y, -1/2+z$	C8-H8...Cg2	3.298	4.099	131.7	
								C17-H17...Cg1	2.936	3.565	117.3	
								C7-H7...C10	2.856	3.536	120.9	
								C16...C3		3.375		1
								C16-H16...H1A-C1	2.230	3.181	145.3	
3	6.235	-0.7	-1.3	-8.3	5.3	-5.1	$x, y, -1+z$	C17-H17...N2	2.622	3.321	121.6	
4	9.599	-1.0	-0.7	-4.1	3.1	-2.7	$-1/2+x, 1/2-y, z$	C14-H14...N2	2.657	3.738	176.0	6
								C14-H14...C11	2.609	3.597	151.4	

^aCentroid-to-centroid distance of molecular pair; Cg1 is the centroids of C3 – C8 ring and Cg2 is the centroids of C12 – C17 ring



1
2
3 **Figure 4.** Selected molecular pairs extracted from the crystal structures of **I** and **II** along with
4
5 their interaction energies (see Table 5).
6
7

8
9 **Hirshfeld surface analysis.** The relative contributions of various intermolecular interactions
10 are quantified using the Hirshfeld surface (HS) diagram and decomposed two-dimensional
11 fingerprint (FP) plot.⁶³⁻⁶⁶ These plots are generated using the CrystalExplorer program, as
12 described previously.⁴⁴ Figure 5 shows the HS diagrams for the crystal structures of **I**, **II** and **A**.
13
14 As noted earlier that the crystal packings are same for **I** and **II**. The decomposed two
15 dimensional fingerprint plots and the relative contributions of various intermolecular contacts
16 present in **I**, **II** and **A** are depicted in Figures 6 and 7, respectively. As expected, the relative
17 contributions of various intermolecular contacts in **I** and **II** are nearly identical. The result
18 suggests that the intermolecular H...H contacts have a major contribution (35.1%) to the crystal
19 packing of **I** and **II**, whereas this contact is slightly higher in **A** (45.5%). Similarly,
20 intermolecular C...H/ H...C contacts are higher in **A** (39.7 %) when compared to **I** (31.1%) and
21 **II** (31.3%). This reduction could be the presence of bromine atom at the para position of phenyl
22 ring. The H...Br contacts contribute 12.6% in **I** and 12.7% in **II**. On the HS diagrams, there is a
23 small difference observed on the surface of methyl groups. This little difference could be the
24 reason for the different charge transfer for the molecule and it could also be explained through
25 different optical properties of crystals **I** and **II**.
26
27
28
29
30
31
32
33
34
35
36
37
38
39
40
41
42
43
44
45
46
47
48
49
50
51
52
53
54
55
56
57
58
59
60

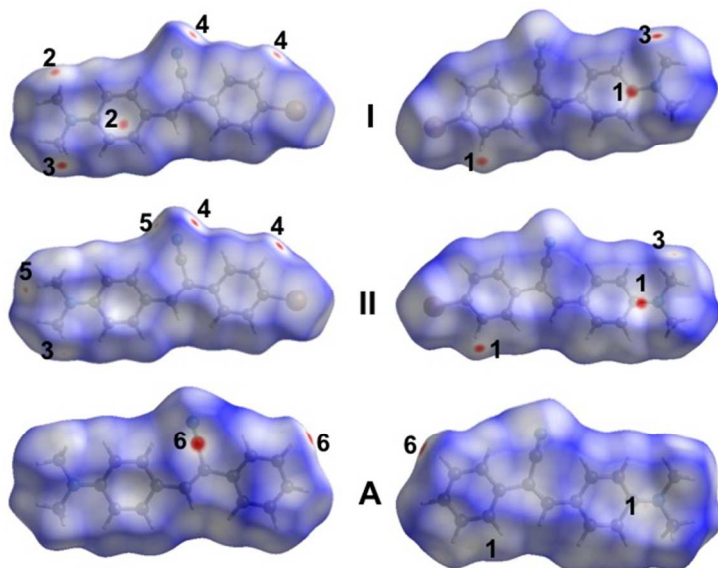


Figure 5. Two different views of the Hirshfeld surfaces mapped with d_{norm} for crystal I, crystal II and compound A. (see Table 5 for the numbering points).

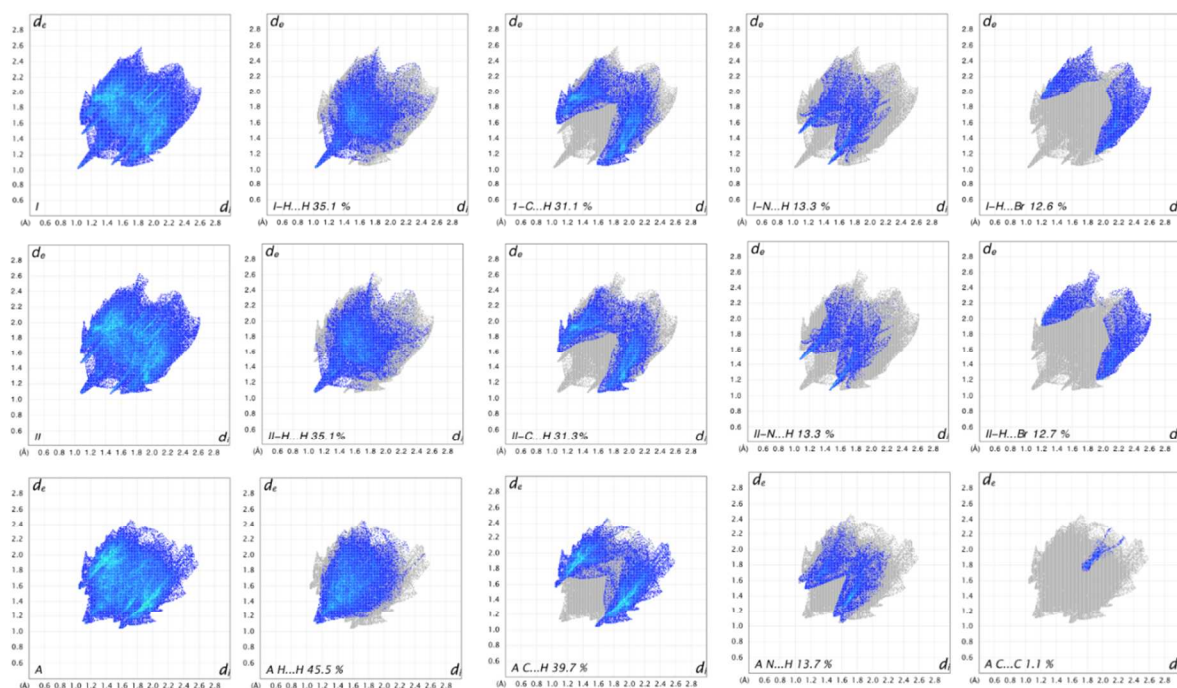


Figure 6. Two-dimensional fingerprint (FP) plots for various intermolecular interactions. The relative contributions of various intermolecular interactions are indicated.

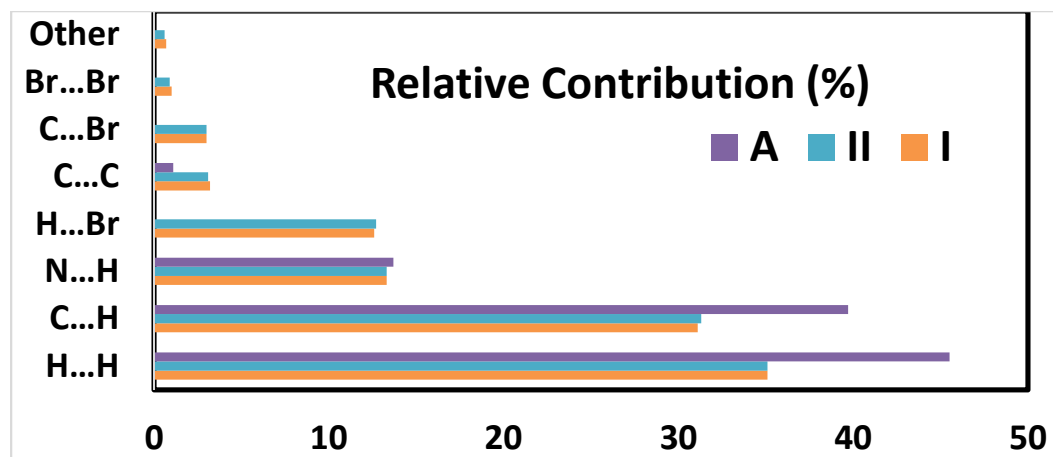


Figure 7. The relative contributions (%) of various intermolecular contacts present in the structures **I**, **II** and **A**.

Optical Characterization in Solution and Solid State. The crystals of **I** are yellow in color, whereas those of **II** are orange. These crystals were characterized by UV-Vis spectroscopy in CHCl_3 solvent and the results indicate that there is a slight variation in the absorption spectra for **I**, **II** and **A** (λ_{max} at 403nm for crystal **I** and at 405 nm for crystal **II**; Figure 8(a). The absorption maxima are assigned to the typical $\pi\text{-}\pi^*$ transition of a conjugated double bond. However, -CN is superior as an electron-withdrawing group. In a related compound, 4-*N,N*-dimethylaminophenylstilbene, λ_{max} is found to be at 347 nm in hexane and at 351 nm in acetonitrile.⁶⁷ A second absorption is observed at approximately 254 nm for **A** (259 nm for **I** and 260 nm for **II**), which corresponds to the $\text{n}\rightarrow\pi^*$ transition due to the amine moiety. A small and invariant absorption band is observed at 328 nm, which may be assigned to the -CN group in **I**, **II** and **A**. It is of interest to note that the absorbance values in solution do not explain the color difference between **I** and **II**.

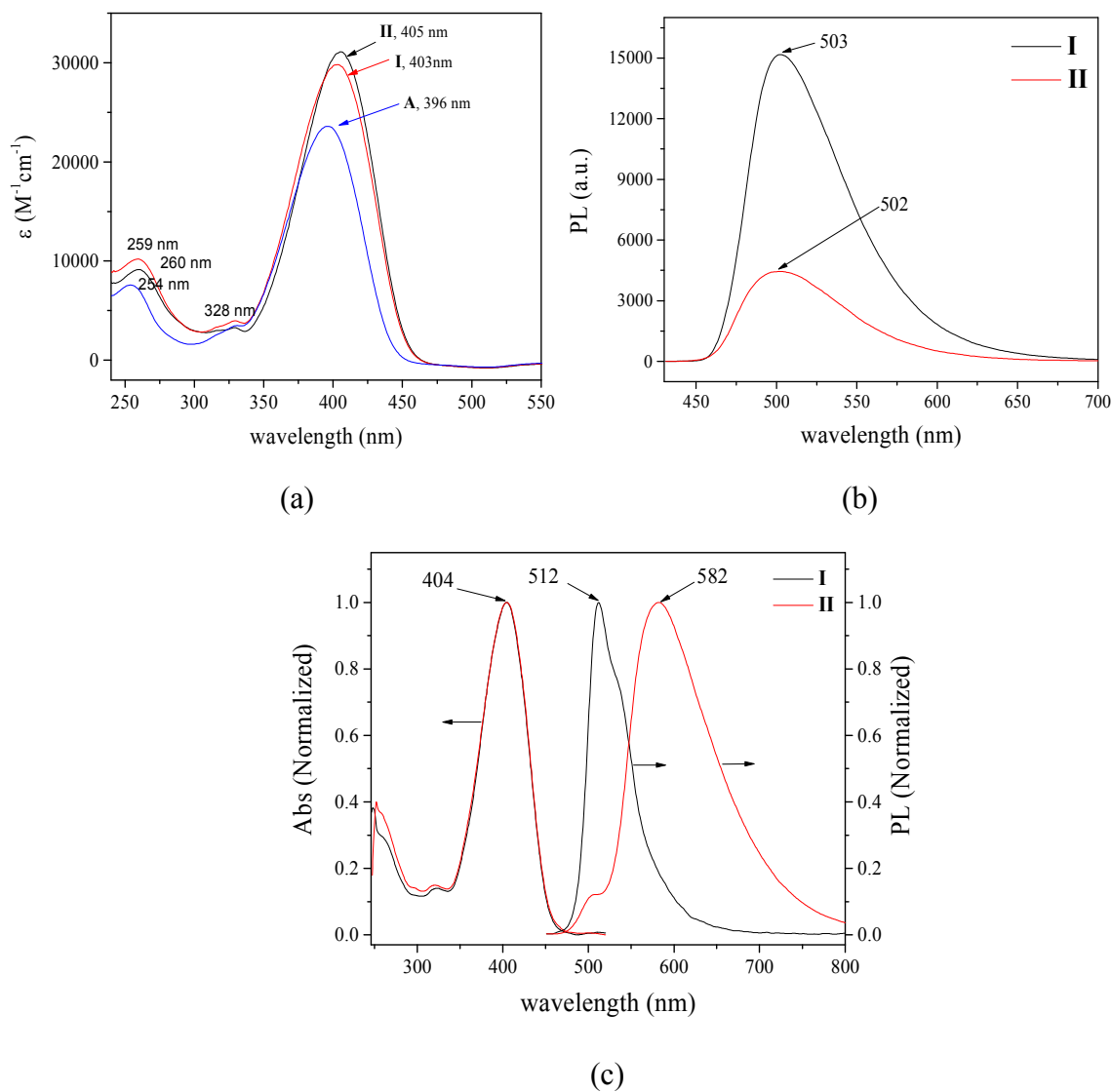


Figure 8. Absorbance spectra of **I**, **II** and **A** in $CHCl_3$ (a), emission spectra of **I** and **II** in $CHCl_3$ (b), and the absorption and emission of **I** and **II** in the solid state (in KBr) (c).

The fluorescence emission spectra of **I** and **II** in solution are displayed in Figure 8(b). From the figure, it can be seen that the PL emission maxima for **I** and **II** are observed at 502 nm and 503 nm (green wavelength), respectively. This clearly indicates a strong redshift, with a Stokes shift ($\Delta\lambda_{st}$) value of 98 nm. No quenching phenomenon is exhibited, as reported for compound **A**³¹. This clearly indicates that the bromine atom may have a possible effect on the structure.

1
2
3 The absorption and emission spectra of **I** and **II** in the solid state are shown in Figure 8(c). The
4
5 results indicate that the absorbance is nearly the same for both **I** and **II** in the solid state. It is
6
7 interesting to see that there is a change in the emission spectra. Crystal **I** shows a maximum of
8
9 λ_{em} at 512 nm, with a shoulder at 534 nm, whereas **II** displays a λ_{em} at 582 nm. Thus, the Stokes
10
11 shift ($\Delta\lambda_{st}$) value is found to be 108 nm for **I** and 178 nm for **II**. Moreover, the crystal **I** has a
12
13 quantum yield (Φ_f) that is markedly different from that of the crystal **II**; the former is 27.5%,
14
15 and the latter is 6.6%.
16
17
18
19

20 The above observations underscore the role of the molecular packing in **I** and **II** on their
21
22 optical properties. Several compounds have been reported to exhibit a strong fluorescence
23
24 dependent on the aggregation state (AIE). However, the effect of molecular packing on the
25
26 emission wavelength is an interesting phenomenon that is distinct from the effect of molecular
27
28 conformation that normally affects the emission.⁶⁸
29
30
31

32 To verify the observed fluorescence behavior, which depends on the solid state and
33
34 morphology of the title compound and is not caused by the presence of any impurity, orange
35
36 crystals of **I*** were obtained from the solvent DMF, as mentioned in the experimental section.
37
38 The comparative fluorescence spectra of **I**, **I*** and **II** are shown in Figure 9. It can be seen that
39
40 the fluorescence changes from green to yellow to orange as a result of the solvent treatment.
41
42 Previous reports⁶⁸ have suggested that these optical characteristics may be caused by changes in
43
44 molecular conformation, but this is not the cause for the optical properties of **I** and **II**.
45
46
47
48
49
50
51
52
53
54
55
56
57
58
59
60

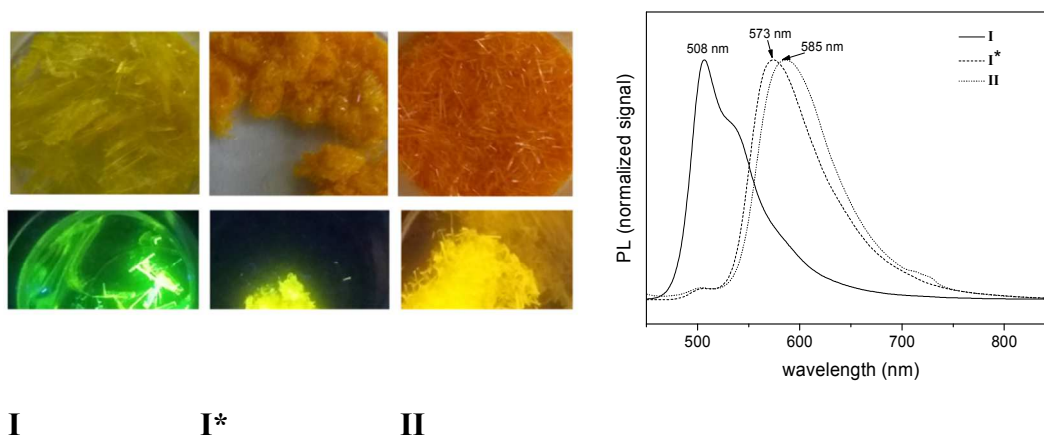


Figure 9. Photographic images showing the crystal habits of **I**, **II**, and the tiny crystals **I***. The emission spectra of **I**, **II** and **I*** and the PL determined for the three types of crystals.

Crystals of **I** and **II** were also characterized by powder X-ray diffraction (PXRD) (Figure 10). The powder XRD patterns are nearly the same for both **I** and **II**. This indicates that both **I** and **II** exist in the same phase. Figure 10 shows that the characteristic peaks for **I** occur at 2θ : 8.16, 15.13, 16.28, 17.22, 19.08, 22.25, 26.76, 24.32, 25.94, 27.43, 32.84 and 49.79° . A minor difference in second decimal places is observed for **II**. However, the intensities of the diffraction peaks are different for both crystals because the total area of each crystal face differs according to the crystal habit.⁶⁹ The experimental powder XRD patterns of **I** and **II** are in good agreement with those of the calculated spectra⁵³ (see S1).

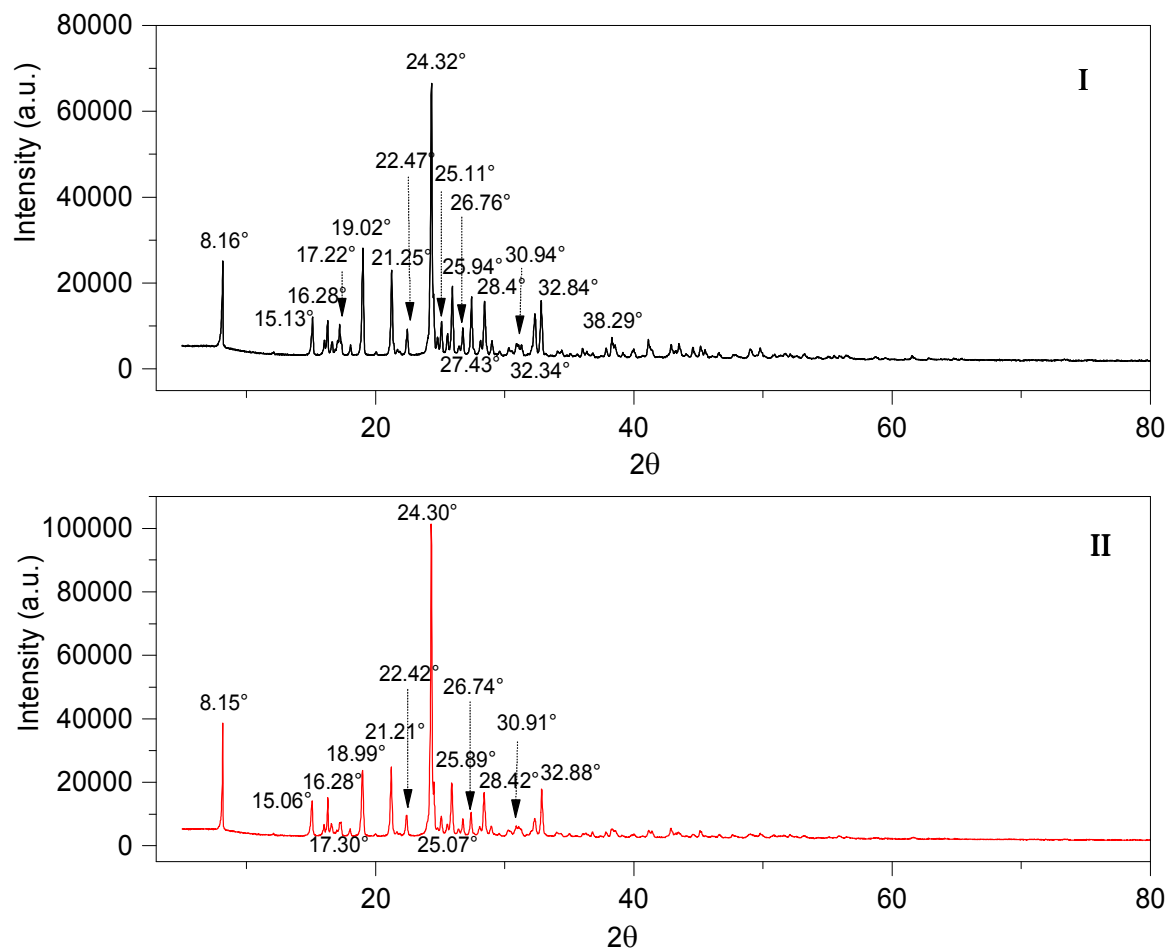
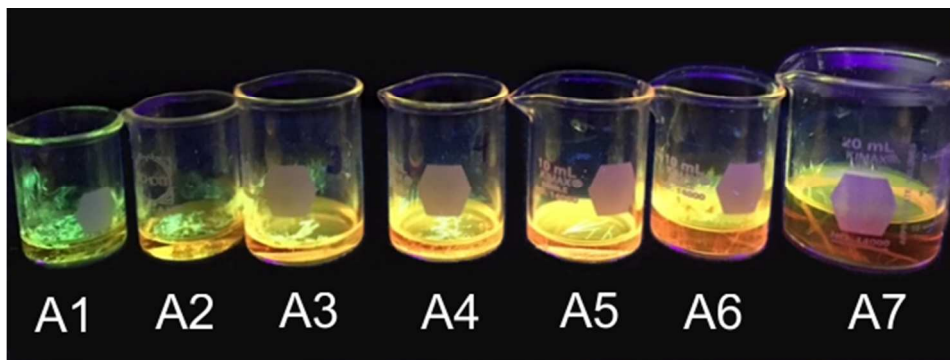


Figure 10. Experimental powder diffraction patterns of **I** and **II**.

The crystal habit differs from the crystal shape, and the results from the different growth rates of each crystal face. The growth rates of equivalent crystal faces can differ according to the reaction conditions, even if the targets are identical substances with the same number of constituent faces. These factors can result in differences of crystal habits; *i.e.*, the crystal shape and crystal size can differ among substances showing different habits. Similar trends of structure-dependent differences in optical properties, as reported herein for compounds **I** and **II**, have been observed in inorganic semiconducting nanoparticles.⁷⁰

The title compound Z-4-BrPhDMAPhACN was dissolved in the solvent DMF and heated at 110 °C for 4 h. From the mixture, aliquots at different time points were collected and kept for

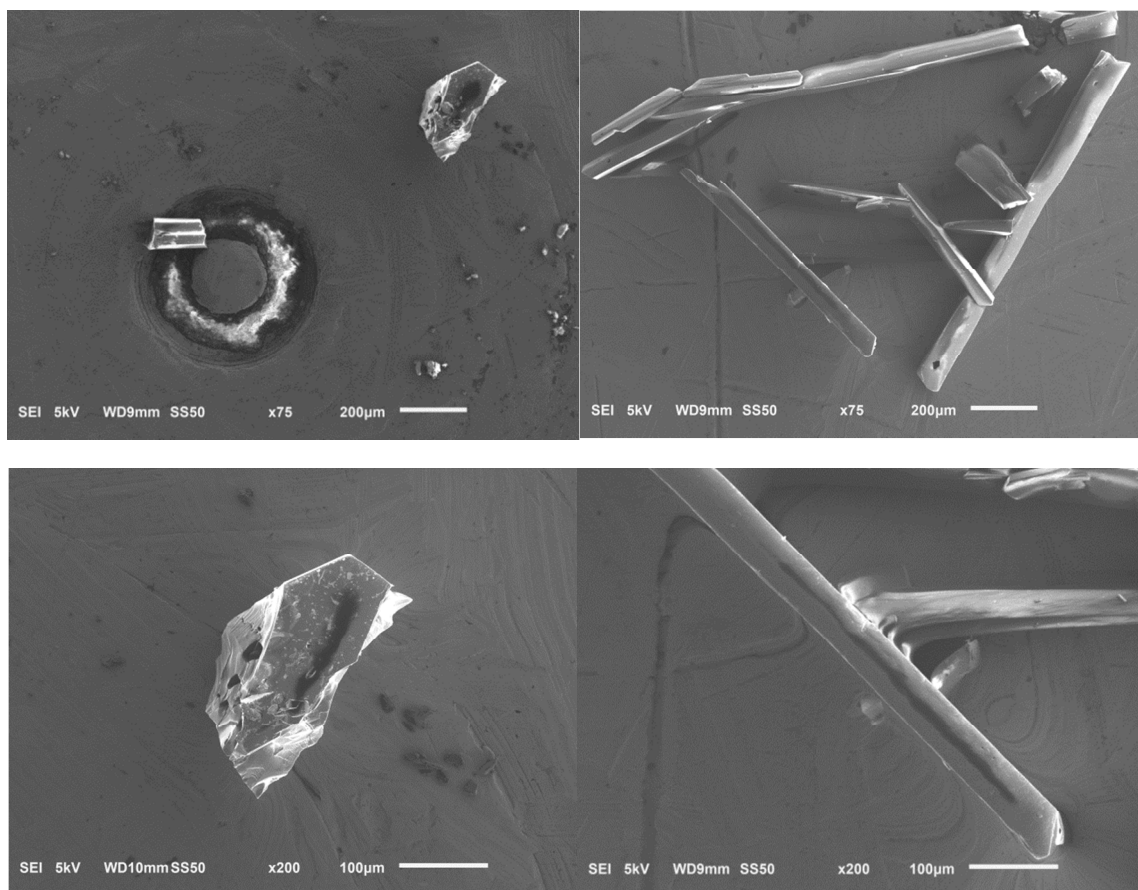
1
2
3 crystallization, as shown in Figure 11. These samples have also been characterized by SCXRD
4
5 and DSC. It can be seen clearly that the color change and fluorescence of the formed crystal
6
7 depend on the duration of solvent treatment. The SCXRD and DSC thermograms collectively
8
9 suggest that the crystals have the same structure. Therefore, the difference in fluorescence
10
11 behavior is independent of the existence of polymorphism (see S1).
12
13
14



15
16
17
18
19
20
21
22
23
24
25
26
27
Figure 11. Crystallization of aliquots separated from the solution: A1 (2 h), A2 (4 h), A3 (6 h),
28
29 A4 (8 h), A5 (10 h), A6 (12 h) and A7 (24 h) under a UV-vis lamp.
30
31
32

33 It is well known that the solvent plays an important role in the crystallization process.⁷¹⁻
34
35
36 ⁷⁵Different solvents often result in different forms of crystal structures and morphologies for the
37
38 same compound. Occasionally, the crystal color that is perceived by the eyes may not provide an
39
40 accurate depiction of the true crystal color. If the mother liquor is colored and the sample is
41
42 dried, then the remaining mother liquor might be deposited on the crystal faces. Scanning
43
44 electron microscopy (SEM) images were acquired for samples **I** and **II** to understand why the
45
46 fluorescence phenomenon is strongly dependent on the morphology. Figure 12 shows the SEM
47
48 images of crystals **I** and **II**. The results indicate that the surface morphology of **I** is block-shaped,
49
50 whereas that of **II** is needle-shaped. Images of the crystals show surface defects that could be
51
52 generated by the solvent used, with lengths up to 10 μm for **I**. It was found that the dispersion of
53
54 defects on the surfaces is narrower in **I** than in **II**. In addition, it was found that the solution
55
56
57
58
59
60

1
2
3 becomes permanently colorless within days after the formation of crystals. This may indicate that
4
5
6 the fluorescing species in nanocrystals of various aging times are the same.
7



37
38
39
40
41
42
43
44
45
46
47
48
49
50
51
52
53
54
55
56
57
58
59
60
(a)

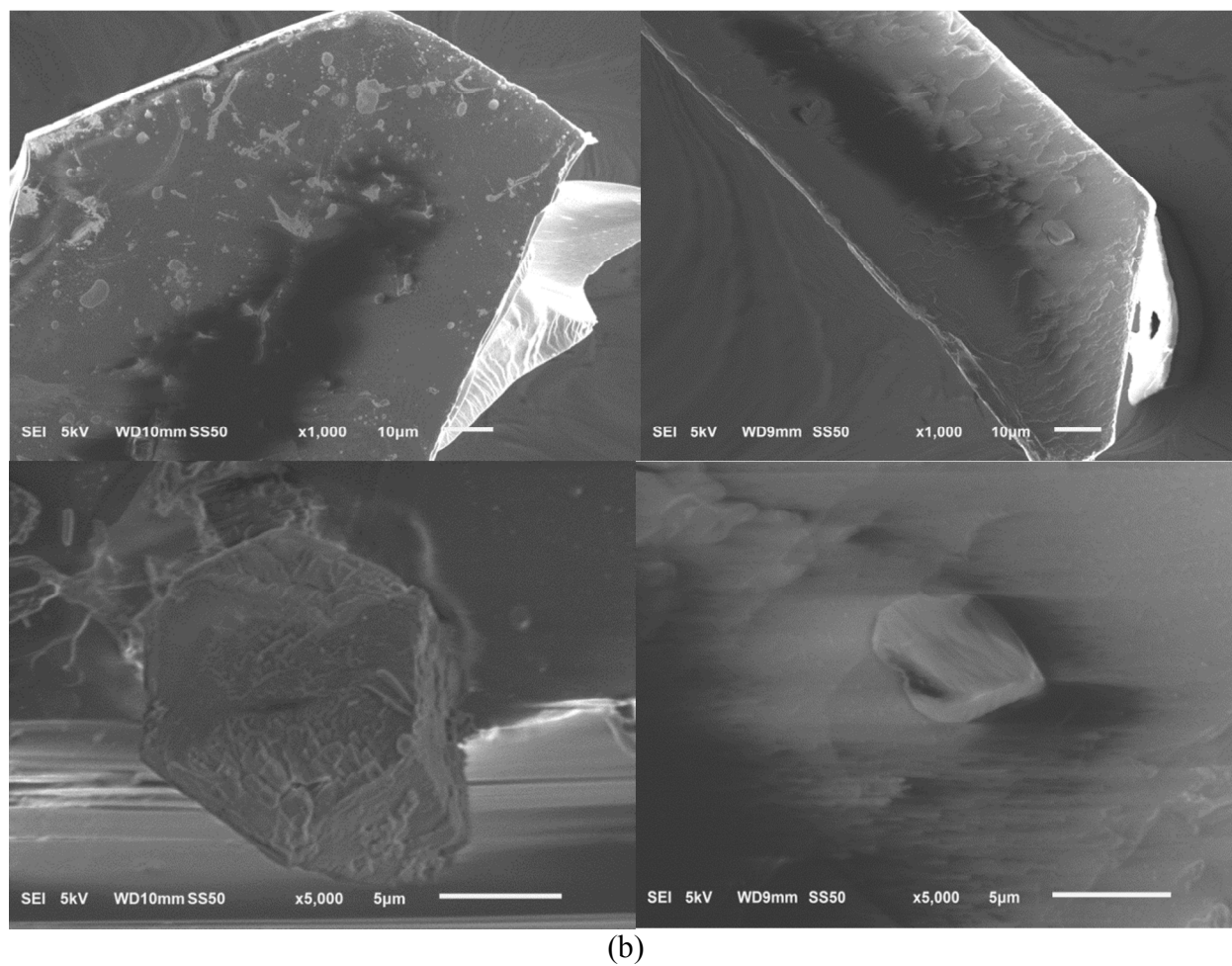
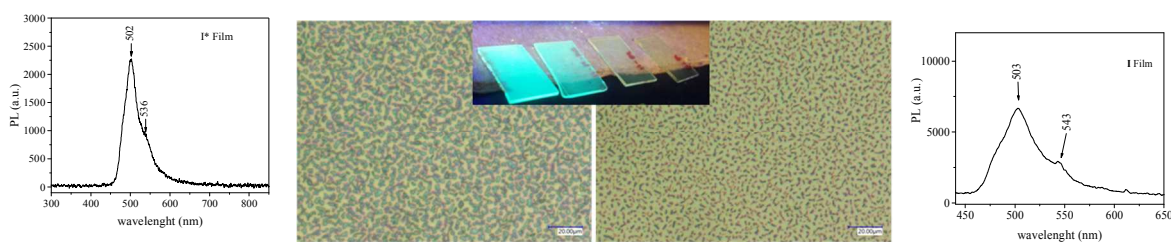


Figure 12. SEM images of crystals of **I** (a) and **II** (b) at different magnifications to observe the effects of different crystallization conditions.

Optical Properties of I, I* and II Based Films. Crystals of **I**, **I*** and **II** were deposited by evaporation under high-vacuum conditions to make films and thereby understand the effect of

1
2
3 deposition on the emission properties. Figure 13 shows that the crystallite sizes for **I** and **I*** are
4
5 different, even when both are deposited in a similar manner. In the case of **I***, the PL spectrum
6
7 measured from the film shows a maximum emission wavelength of 502 nm. The PL spectra were
8
9 also measured directly from the crystal of **I***. This spectrum shows two bands at 503 and 551
10
11 nm. It is interesting to note that the former band is also observed in solution (see Figure 8(b)). In
12
13 the case of **I**, the PL spectra show a wide band with an emission at 517 nm and a shoulder at 543
14
15 nm. The latter is present in both film-based measurements and direct measurements on the
16
17 crystal. Furthermore, the intensity decreases in the case of film-based experiments. This decrease
18
19 in intensity could be due to the crystallite size (tiny). The ratio of the two emission bands is
20
21 affected by the crystallite size. This indicates possible electronic effects, such as charge transfer
22
23 between molecules in the crystals. Similarly, PL spectra were measured for a film and crystal of
24
25 **II** (Figure 14). The PL spectrum of the film of **II** shows two maxima at 503 nm and 548 nm. This
26
27 result indicates that two kinds of crystals, **II** and **I**, are present, regardless of the deposition
28
29 conditions.
30
31
32
33
34
35



(a)



(b)

Figure 13. Nanocrystals of **I** and **I*** after deposition at high vacuum and PL spectra of their films under a UV source (a) and PL spectra of the crystals of **I*** and **I** (b).

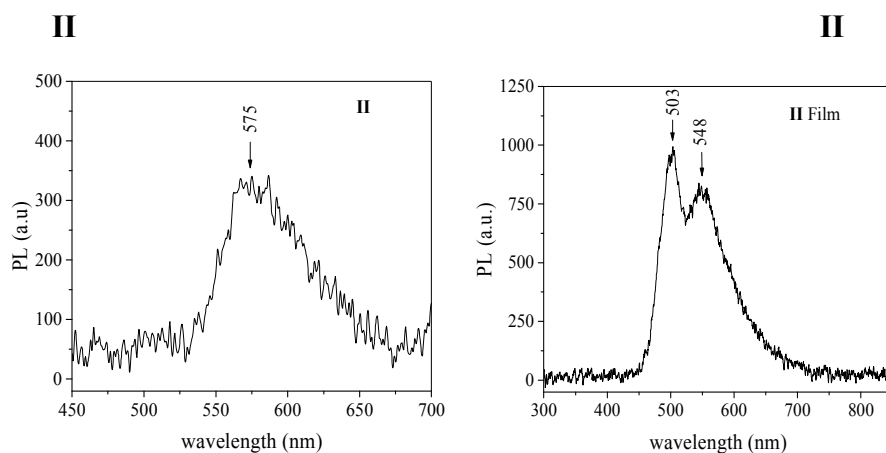
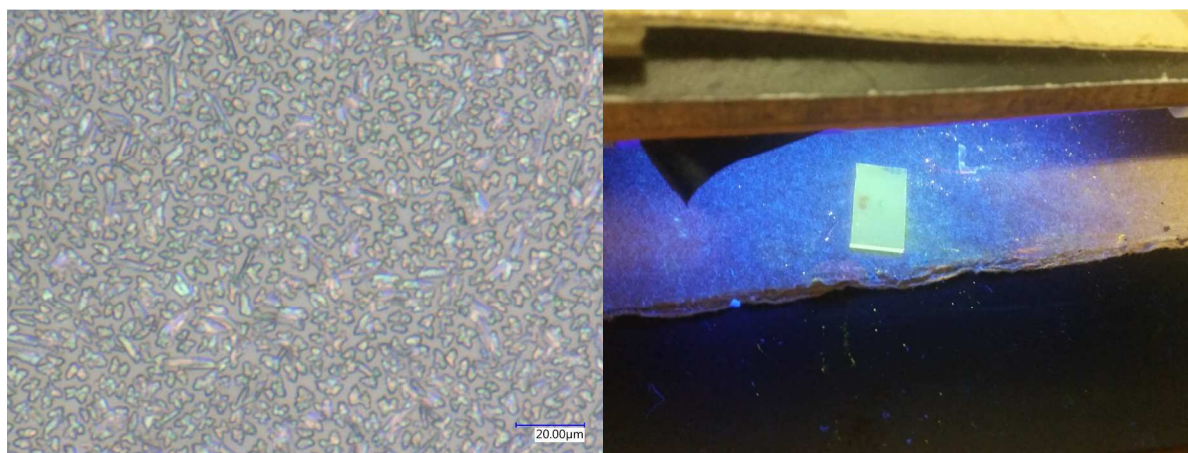


Figure 14. Nanocrystals of **II** deposited by evaporation under high-vacuum conditions. Left: PL spectrum of a crystal; right: PL spectrum of a film.

The electrochemical characteristics of samples **I**, **II** and **A** were investigated by cyclic voltammetry (CV) (Figure 15). The onset oxidation potentials ($E_{\text{Ox}}^{\text{onset}}$), as estimated from the CV curves for **I**, **II** and **A**, are 0.9055, 0.9236, and 0.904 V, respectively. In addition, the onset reduction potentials ($E_{\text{Red}}^{\text{onset}}$) estimated from the CV curves for **I**, **II** and **A** are -0.86805, -0.8533, and -0.835 V, respectively. The HOMO and LUMO energy levels of the samples were calculated from the CV tests, using formulas reported previously.⁷⁶

$$HOMO = -(E_{ox} - E_{1/2(ferrocene)} + 4.8eV)$$

$$LUMO = -(E_{red} - E_{1/2(ferrocene)} + 4.8eV)$$

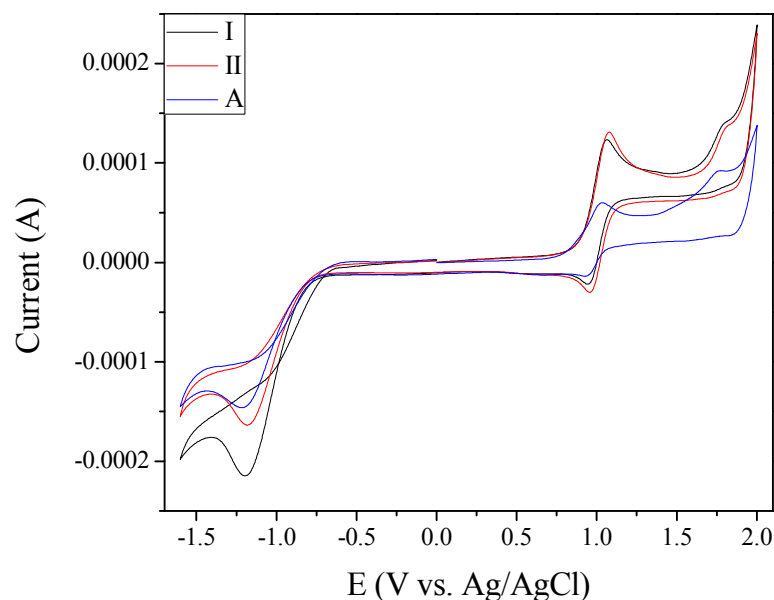


Figure 15. Cyclic voltammograms of **I**, **II** and **A** in 1 mM 0.1 M TBAFP₆/CH₂Cl₂ solution, using Ag/AgCl as the reference electrode and Pt wire as the working electrode. A scan rate of 50 mVs⁻¹ was used.

The value of **A**, which has a lower-energy HOMO level than do **I** and **II**, indicates that the **A** group has a stronger tendency to donate an electron, whereas the high LUMO energy level of **II** indicates its strong electron-withdrawing ability, as shown in Table 6.

Table 6. Electrochemical characteristics and HOMO–LUMO energy values for **I**, **II** and **A**

	Experimental				Calculated		
	E _{Ox} ^{onset} (V)	E _{Red} ^{onset} (V)	HOMO (eV)	LUMO (eV)	HOMO (eV)	LUMO (eV)	ΔE=LUMO – HOMO(eV)
I	0.9055	-0.86805	-5.2058	-3.4322	-7.7566	-5.6194	2.1371
II	0.9236	-0.8533	-5.2239	-3.4470			
A	0.904	-0.8350	-5.168	-3.4290	-6.5579	-1.0656	5.4924

The optical properties are generally governed by the composition of the frontier molecular orbitals and the HOMO and LUMO energy levels, as shown in Figure 16. The HOMO orbitals

are localized over the 4-*N,N*-dimethylaminophenyl rings, whereas the LUMO orbitals are localized over the (–C=C–CN) cyano group and 4-bromophenyl ring of the title compound (Figure 16). The simulated absorbance spectra show an intense absorbance at 375 nm (in CHCl₃, the oscillator strength is 1.3199) and 346 nm (in the gaseous state, the oscillator strength is 1.1707), which are mainly due to the transfer of charge from the HOMO orbital to the LUMO orbital (97% contribution). Other possible transitions are listed in Table 7. Furthermore, emissions for similar transitions were observed at 533 nm (in CHCl₃, the oscillator strength is 1.1475) and 479 nm (in the gaseous state, the oscillator strength is 0.8611). The experimental absorbance and emission transitions and the corresponding values calculated from DFT method are in good agreement. The HOMO – LUMO bond gap energy is compared with that of compound A. The energy difference is very low in crystal I ($\Delta E = 2.1371$ eV), but it is high in compound A ($\Delta E = 7.0398$ eV). These results suggest that the bromine atom substitution in the title compound facilitates the charge transfer transition in this compound.

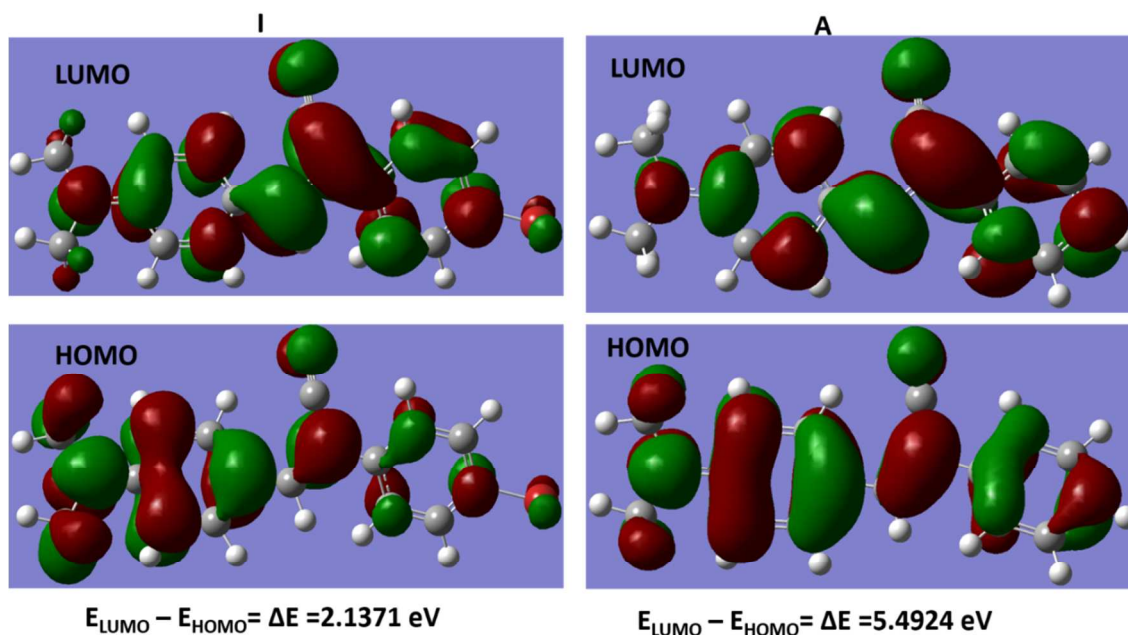


Figure 16. HOMO and LUMO orbitals of I and A.

Table 7. Calculated absorption energies (λ), emission wavelengths (λ) and oscillatory strengths (f) of **I**, **II** and **A** using M062X/cc-pVTZ level theory

Absorption				Emission			
$\lambda_{\text{abs.}}$ (Cal. nm)	f	Orbital contribution	λ_{abs} (Exp. nm)	$\lambda_{\text{em.}}$ (Cal. nm)	f	Orbital contribution	$\lambda_{\text{em.}}$ (Exp. nm)
I and II							
375.35 ^a	1.3199	H → L (97%)	404 ^a	533.32 ^a	1.1475	H → L (98%)	502 ^a
275.70 ^a	0.0519	H-2 → L (15%) H → L+2 (49%) H → L+3 (29%)		292.27 ^a	0.1027	H-1 → L (90 %) H → L+1 (4%)	
253.75 ^a	0.07	H-1 → L (69%) H → L+1 (13%) H-1 → L+1(5%)		257.49 ^a	0.3094	H-3 → L (18%) H → L+3 (65%) H → L+2 (8%)	
345.46 ^b	1.1707	H → L (97%)		479	0.8611	H → L (99%)	502 ^a
A							
361.56 ^a	1.1871	H → L (97%)	381 ^a	537.68 ^a	1.0106	H → L (99%)	-
272.98 ^a	0.0603	H-3 → L (12%) H → L+1 (19%) H → L+2 (61%)		290.075 ^a	0.1339	H-1 → L (90%) H → L+1 (5%)	
248.42 ^a	0.0023	H-2 → L (22%) H-1 → L (17%) H-1 → L+1(12%) H → L+1 (27%)		254.01 ^a	0.1768	H-3 → L (72%) H → L+1 (15%) H->L+3 (7%)	

^aoptical properties in solution state and ^boptical properties in gas state

CONCLUSION

(2Z)-2-(4-bromophenyl)-3-[4-(dimethylamino)phenyl]prop-2-enitrile, as reported here, was prepared and characterized by ¹H-NMR, EI, FT-IR, UV-Vis spectroscopy, fluorescence, CV, single-crystal/powder XRD, DSC and SEM. Crystals with the obtained morphology and size exhibit enhanced emission compared to the same concentration of ions dissolved in a good solvent. The enhanced emission is considered to be the result of the variation of intra- and intermolecular interactions with solvents such as DMSO and DMF. The crystallization process of **I** and **II** was studied, which indicated that its transformation depends on the solvent used and time. In contrast, large numbers of uniform crystals can be obtained by improving the experimental conditions to investigate the property-structure relationships. The crystal habit and color of the

1
2
3 crystals provide an opportunity to study this compound under varying conditions, such as with
4
5 varying solvents and at various temperatures, to determine the thermodynamic properties of the
6
7 crystallization process. The crystal structures of **I**, **II** and **A** have been analyzed using Hirshfeld
8
9 surfaces and the PIXEL energy calculations. The optimized structures of these compounds in the
10
11 gas phase are superimposed well and there is no detectable changes observed. Further, the
12
13 HOMO and LUMO energies are derived from the experimental and computational methods.
14
15 Therefore, identifying the source of the optical differences could extend our knowledge in an
16
17 area of research that follows a well-established tradition in solid-state chemistry. The complexity
18
19 of this problem is well captured by the fact that although there have been many studies, this
20
21 problem has not been solved fully. However, predictions may be possible using experimental and
22
23 theoretical approaches in organic solid-state chemistry that consider the nanoparticle properties.
24
25 We think that this phenomenon, which was observed clearly during the crystallization and
26
27 growth of microcrystals, can be used for nanoscale electronic devices and is related to electron
28
29 conduction.
30
31
32
33
34
35

36 ASSOCIATED CONTENT

37
38
39 **Supporting information S1.** Preparation of crystals, NMR, IR and mass spectra, vibrational
40
41 frequencies, bond lengths and torsion, simulated powder diffraction patterns, and thermograms.
42
43
44

45 Accession codes

46
47
48 The crystallographic data (excluding structure factors) reported in this paper have been deposited
49
50 with the Cambridge Crystallographic Data Centre as supplementary publication no. CCDC
51
52 1439756 and 1439757. Copies of the available material can be obtained, free of charge, on
53
54
55
56
57
58
59
60

1
2
3 application to the CCDC, 12 Union Road. Cambridge CB2 IEZ, UK, (fax: +44-(0)1223-336033
4
5 or e-mail: deposit@ccdc.cam.ac.uk).
6
7

8 9 AUTHOR INFORMATION

10
11 Corresponding Author

12
13 judith.percino@correo.buap.mx
14
15
16

17
18 Notes

19
20
21 The authors have no conflicts of interest to declare
22

23 24 ACKNOWLEDGMENTS

25
26 The authors wish to express their gratitude to VIEP-BUAP (project PEZM-NAT16-G),
27
28 PROMEP-SEP/103.5/13/2110 (Thematic network of collaboration) and CONACyT (Programa
29
30 Cátedras para Jóvenes Investigadores), as well as to F. E. Longoria Rodriguez (CIMAV-MTY)
31
32 and Vladimir Carranza for technical assistance with XRD and mass spectrometry, respectively.
33
34
35 The authors would also like to thank Laboratorio Nacional de Supercómputo del Sureste (LNS-
36
37 BUAP) for the calculus service.
38
39
40
41
42
43
44
45
46
47
48
49
50
51
52
53
54
55
56
57
58
59
60

REFERENCES

- (1) Brittain, H. G.; Byrn, S. R.; Lee, E. In *Structural Aspects of Polymorphism*; Brittain, H. G., Ed.; Inform Healthcare: New York, 2009; Vol. 192, pp 185–230.
- (2) Katrincic, L. M.; Sun, Y. T.; Carlton, R. A.; Diederich, A. M.; Mueller, R. L.; Vogt, F. G. *Int. J. Pharm.* **2009**, *366*, 1–13. Characterization, selection, and development of an orally dosed drug polymorph from an enantiotropically related system.
- (3) Byrn, S. R.; Pfeiffer, R. R.; Stephenson, G.; Grant, D. J. W.; Gleason, W. B. *Chem. Mater.* **1994**, *6*, 1148–1158. Solid-state pharmaceutical chemistry.
- (4) Picker-Freyer, K. M.; Liao, X.; Zhang, G.; Wiedmann, T. S. *J. Pharm. Sci.* **2007**, *96*, 2111–2124. Evaluation of the compaction of sulfathiazole polymorphs.
- (5) Bernstein, J. *J. Phys. D: Appl. Phys.* **1993**, *26*, B66–B76. Crystal growth, polymorphism and structure-property relationships in organic crystals.
- (6) Tong, L.; Gattass, R. R.; Ashcom, J. B.; He, S.; Lou, J.; Shen, M.; Maxwell, I.; Mazur, E. *Nature* **2003**, *426*, 816–819. Subwavelength-diameter silica wires for low-loss optical wave guiding.
- (7) Braga, D.; Grepioni, F.; Maini, L. *Chem. Commun.* **2010**, *46*, 6232–6242. The growing world of crystal forms.
- (8) Zhang, R.; Zhang, Q.; Liu, Z.; Yang, L.; Wu, J.; Zhou, H.; Yang, J.; Tian, Y. *CrystEngComm* **2014**, *16*, 2039–2044. Two polymorphs and cocrystal of styryl-pyridine derivatives with tuned emission induced by Co^{2+} and $\text{Zn}(\text{phen})_3^{2+}$.

1
2
3 (9) Yoon, S.-J.; Park, S. *J. Mater. Chem.* **2011**, *21*, 8338–8346. Polymorphic and
4
5
6
7
8
9
10
11
12
13
14
15
16
17
18
19
20
21
22
23
24
25
26
27
28
29
30
31
32
33
34
35
36
37
38
39
40
41
42
43
44
45
46
47
48
49
50
51
52
53
54
55
56
57
58
59
60

mechanochromic luminescence modulation in the highly emissive dicyanodistyrylbenzene crystal: secondary bonding interaction in molecular stacking assembly.

(10) Kim, M.; Whang, D. R.; Gierschner, J.; Park, S. Y. *J. Mater. Chem. C* **2015**, *3*, 231–234.
A distyrylbenzene based highly efficient deep red/near-infrared emitting organic solid.

(11) Burroughes, J. H.; Bradley, D. D. C.; Brown, A. R.; Marks, R. N.; Mackay, K.; Friend, R. H.; Burns, P. L.; Holmes, A. B. *Nature* **1990**, *347*, 539–541. Light-emitting diodes based on conjugated polymers.

(12) Yamaguchi, Y.; Ochi, T.; Miyamura, S.; Tanaka, T.; Kobayashi, S.; Wakamiya, T.; Matsubara, Y.; Yoshida, Z. I. *J. Am. Chem. Soc.* **2006**, *128*, 4504–4505. Rigid molecular architectures that comprise a 1,3,5-trisubstituted benzene core and three oligoaryleneethynylene arms: light-emitting characteristics and π conjugation between the arms.

(13) Strassert, C. A.; Chien, C.-H.; Galvez Lopez, M. D.; Kourkoulos, D.; Hertel, D.; Meerholz, K.; DeCola, L. *Angew. Chem., Int. Ed.* **2011**, *50*, 946–950. Switching on luminescence by the self-assembly of a platinum(II) complex into gelating nanofibers and electroluminescent films.

(14) O'Neill, M.; Kelly, S. M. *Adv. Mater.* **2003**, *15*, 1135–1146. Liquid crystals for charge transport, luminescence, and photonics.

(15) Fischer, M. K.; Wenger, S.; Wang, M.; Mishra, A.; Zakeeruddin, S. M.; Grätzel, M.; Bäuerle, P. *Chem. Mater.* **2010**, *22*, 1836–1845. D- π -A sensitizers for dye-sensitized solar cells: linear vs branched oligothiophenes.

1
2
3 (16) Cai, N.; Moon, S. J.; Cevey-Ha, L.; Moehl, T.; Humphry-Baker, R.; Wang, P.;
4
5 Zakeeruddin, S. M.; Gratzel, M. *Nano Lett.* **2011**, *11*, 1452–1456. An organic D- π -A dye for
6
7 record efficiency solid-state sensitized heterojunction solar cells.
8
9

10
11 (17) Wong, K. L.; Law, G. L.; Yang, Y. Y.; Wong, W. T. *Adv. Mater.* **2006**, *18*, 1051–1054. A
12
13 highly porous luminescent terbium–organic framework for reversible anion sensing.
14
15

16
17 (18) Liu, H.; Mack, J.; Guo, Q.; Lu, H.; Kobayashi, N.; Shen, Z. *Chem. Commun.* **2011**, *47*,
18
19 12092–12094. A selective colorimetric and fluorometric ammonium ion sensor based on the H-
20
21 aggregation of an aza-BODIPY with fused pyrazine rings.
22
23

24
25 (19) Yan, D.; Lu, J.; Ma, J.; Wei, M.; Evans, D. G.; Duan, X. *Angew. Chem., Int. Ed.* **2011**, *50*,
26
27 720–723. Reversibly thermochromic, fluorescent ultrathin films with a supramolecular
28
29 architecture.
30
31

32
33 (20) Yan, D.; Delori, A.; Lloyd, G. O.; Frišćić, T.; Day, G. M.; Jones, W.; Lu, J.; Wei, M.;
34
35 Evans, D. G.; Duan, X. *Angew. Chem., Int. Ed.* **2011**, *50*, 12483–12486. A cocrystal strategy to
36
37 tune the luminescent properties of stilbene-type organic solid-state materials.
38
39

40
41 (21) Dong, B.; Wang, M.; Xu, C.; Feng, Q.; Wang, Y. *Cryst. Growth Des.* **2012**, *12*, 5986–
42
43 5993. Tuning solid-state fluorescence of a twisted π -conjugated molecule by regulating the
44
45 arrangement of anthracene fluorophores.
46
47

48
49 (22) Lehmann, C. W. *Angew. Chem., Int. Ed.* **2011**, *50*, 5616–5617. Crystal structure
50
51 prediction—dawn of a new era.
52
53
54
55
56
57
58
59
60

1
2
3 (23) Zhang, G.; Lu, J.; Sabat, M.; Fraser, C. L. *J. Am. Chem. Soc.* **2010**, *132*, 2160–2162.
4
5 Polymorphism and reversible mechanochromic luminescence for solid-state difluoroboron
6
7
8 avobenzene.
9

10
11 (24) Zhang, H. Y.; Zhang, Z. L.; Ye, K. Q.; Zhang, J. Y.; Wang, Y. *Adv. Mater.* **2006**, *18*,
12
13 2369–2372. Organic crystals with tunable emission colors based on a single organic molecule
14
15 and different molecular packing structures.
16
17

18
19 (25) Hong, Y.; Lam, J. W. Y.; Tang, B. Z. *Chem. Soc. Rev.* **2011**, *40*, 5361–5388.
20
21 Aggregation-induced emission.
22
23

24
25 (26) An, B. K.; Kwon, S. K.; Jung, S. D.; Park, S. Y. *J Am Chem Soc* **2002**, *124*, 14410–14415.
26
27 Enhanced emission and its switching in fluorescent organic nanoparticles.
28
29

30
31 (27) Li, Z.; Dong, Y. Q.; Lam, J. W. Y.; Sun, J.; Qin, A.; Häußler, M.; Dong, Y. P.; Sung, H.
32
33 H. Y.; Williams, I. D.; Kwok, H. S.; Tang, B. Z. *Adv. Funct. Mater.* **2009**, *19*, 905–917.
34
35 Functionalized siloles: versatile synthesis, aggregation-induced emission, and sensory and device
36
37 applications.
38
39

40
41 (28) Zhang, X.; Chi, Z.; Li, H.; Xu, B.; Li, X.; Liu, S.; Zhang, Y.; Xu, J. *J. Mater. Chem.* **2011**,
42
43 *21*, 1788–1796. Synthesis and properties of novel aggregation-induced emission compounds with
44
45 combined tetraphenylethylene and dicarbazolyl triphenylethylene moieties.
46
47

48
49 (29) Zhang, G. F.; Aldred, M. P.; Gong, W. L.; Li, C.; Zhu, M. Q. *Chem. Commun.* **2012**, *48*,
50
51 7711–7713. Utilising tetraphenylethene as a dual activator for intramolecular charge transfer and
52
53 aggregation induced emission.
54
55
56
57
58
59
60

1
2
3 (30) Chung, J. W.; Yoon, S. J.; An, B. K.; Park, S. Y. *J. Phys. Chem. C* **2013**, *117*, 11285–
4 11291. High-contrast on/off fluorescence switching via reversible E–Z isomerization of
5 diphenylstilbene containing the α -cyanostilbenic moiety.
6
7

8
9
10 (31) Liang, J.; Chen, Z.; Yin, J.; Yu, G.-A.; Liu, S. H. *Chem. Commun.* **2013**, *49*, 3567–3569.
11 Aggregation-induced emission (AIE) behavior and thermochromic luminescence properties of a
12 new gold(I) complex.
13
14

15
16 (32) Percino, M. J.; Chapela, V. M.; Cerón, M.; Soriano-Moro, G.; Castro, M. E.; Melendez, F.
17 *J. J. Mol. Struct.* **2013**, *1034*, 238–248. Fluorescence improvement of pyridylacrylonitrile by
18 dimethylaminophenyl-substitutions: The effect of packing modes of conjugated compounds.
19
20

21 (33) Palakollu, V.; Kanvah, S. *New J. Chem.* **2014**, *38*, 5736–5746. α -Cyanostilbene based
22 fluorophores: aggregation-induced enhanced emission, solvatochromism and the pH effect.
23
24

25
26 (34) Shan, G. G.; Li, H. B.; Qin, J. S.; Zhu, D. X.; Liao, Y.; Su, Z. M. *Dalton Trans.* **2012**, *41*,
27 9590–9593. Piezochromic luminescent (PCL) behavior and aggregation-induced emission (AIE)
28 property of a new cationic iridium(III) complex.
29
30

31 (35) Xu, B.; Xie, M.; He, J.; Xu, B.; Chi, Z.; Tian, W.; Jiang, L.; Zhao, F.; Liu, S.; Zhang, Y.;
32 Xu, Z.; Xu, J. *Chem. Commun.* **2013**, *49*, 273–275. An aggregation-induced emission
33 luminophore with multi-stimuli single- and two-photon fluorescence switching and large two-
34 photon absorption cross section.
35
36
37
38

39 (36) Shen, X. Y.; Wang, Y. J.; Zhao, E.; Yuan, W. Z.; Liu, Y.; Lu, P.; Qin, A.; Ma, Y.; Sun, J.
40 Z.; Tang, B. Z. *J. Phys. Chem. C* **2013**, *117*, 7334–7347. Effects of Substitution with Donor–
41
42
43
44
45
46
47
48
49
50

1
2
3 Acceptor Groups on the Properties of Tetraphenylethene Trimer: Aggregation-Induced Emission,
4
5 Solvatochromism, and Mechanochromism.
6
7

8
9 (37) Yuan, W. Z.; Tan, Y.; Gong, Y.; Lu, P.; Lam, J. W. Y.; Shen, X. Y.; Feng, C.; Sung, H. H.
10
11 Y.; Lu, Y.; Williams, I. D.; Sun, J. Z.; Zhang, Y.; Tang, B. Z. *Adv. Mater.* **2013**, *25*, 2837–2843.
12
13 Synergy between twisted conformation and effective intermolecular interactions: strategy for
14
15 efficient mechanochromic luminogens with high contrast.
16
17

18
19 (38) Kurita, M.; Momma, M.; Mizuguchi, K.; Nakano, H. *ChemPhysChem* **2013**, *14*, 3898–
20
21 3901. Fluorescence color change of aggregation-induced emission of 4-[Bis(4-
22
23 methylphenyl)amino]benzaldehyde.
24
25

26
27 (39) Sheldrick, G. *Acta Crystallogr., Sect. A* **2008**, *64*, 112–122. A short history of SHELX.
28
29

30
31 (40) de Mello, J. C.; Wittmann, H. F.; Friend, R. H. *Adv. Mater.* **1997**, *9*, 230–232. An
32
33 improved experimental determination of external photoluminescence quantum efficiency.
34
35

36
37 (41) Frisch, M. J.; Trucks, G. W.; Schlegel, H. B.; Scuseria, G. E.; Robb, M. A.; Cheeseman, J.
38
39 R.; Scalmani, G.; Barone, V.; Mennucci, B.; Petersson, G. A.; Nakatsuji, H.; Caricato, M.; Li,
40
41 X.; Hratchian, H. P.; Izmaylov, A. F.; Bloino, J.; Zheng, G.; Sonnenberg, J. L.; Hada, M.; Ehara,
42
43 M.; Toyota, K.; Fukuda, R.; Hasegawa, J.; Ishida, M.; Nakajima, T.; Honda, Y.; Kitao, O.;
44
45 Nakai, H.; Vreven, T.; Montgomery, J. A. J.; Peralta, J. E.; Ogliaro, F.; Bearpark, M.; Heyd, J. J.;
46
47 Brothers, E.; Kudin, K. N.; Staroverov, V. N.; Kobayashi, R.; Normand, J.; Raghavachari, K.;
48
49 Rendell, A.; Burant, J. C.; Iyengar, S. S.; Tomasi, J.; Cossi, M.; Rega, N.; Millam, J. M.; Klene,
50
51 M.; Knox, J. E.; Cross, J. B.; Bakken, V.; Adamo, C.; Jaramillo, J.; Gomperts, R.; Stratmann, R.
52
53 E.; Yazyev, O.; Austin, A. J.; Cammi, R.; Pomelli, C.; Ochterski, J. W.; Martin, R. L.;
54
55 Morokuma, K.; Zakrzewski, V. G.; Voth, G. A.; Salvador, P.; Dannenberg, J. J.; Dapprich, S.;

1
2
3 Daniels, A. D.; Farkas, Ö.; Foresman, J. B.; Ortiz, J. V.; Cioslowski, J.; Fox, D. J. Gaussian, Inc.,
4 Wallingford CT, **2009**.

5
6
7
8
9 (42) Kohn, W.; Sham, L. J. *Phys. Rev.* **1965**, *140*, A1133–A1138. Self-consistent equations
10 including exchange and correlation effects.

11
12
13
14 (43) Wolff, S. K.; Grimwood, D. J.; McKinnon, J. J.; Turner, M. J.; Jayatilaka, D.; Spackman,
15 M. A. *CrystalExplorer (Version 3.0)*; University of Western University of Western Australia:
16 Australia, 2012.

17
18
19
20
21
22 (44) Venkatesan, P.; Thamocharan, S.; Kumar, R. G.; Ilangoan, A. *CrystEngComm* **2015**, *17*,
23 904–915. Invariant and variable intermolecular interactions in functionalized malonic acid half-
24 esters: X-ray, Hirshfeld surface and PIXEL energy analyses.

25
26
27
28
29
30 (45) Reichardt, C. *Green Chem.* **2005**, *7*, 339–351. Polarity of ionic liquids determined
31 empirically by means of solvatochromic pyridinium N-phenolate betaine dyes

32
33
34
35
36 (46) Kleinpeter, E.; Klod, S.; Rudolf, W.-D. *J. Org. Chem.* **2004**, *69*, 4317–4329. Electronic
37 State of Push–Pull Alkenes: An experimental dynamic NMR and theoretical ab initio MO study.

38
39
40
41 (47) Forni, A.; Destro, R. *Chem. - Eur. J.* **2003**, *9*, 5528–5537. Electron density investigation
42 of a push–pull ethylene (C₁₄H₂₄N₂O₂·H₂O) by X-ray Diffraction at T = 21 K.

43
44
45
46
47 (48) Ababneh-Khasawneh, M.; Fortier-McGill, B. E.; Occhionorelli, M. E.; Bain, A. D. *J.*
48 *Phys. Chem. A* **2011**, *115*, 7531–7537. Solvent effects on chemical exchange in a push–pull
49 ethylene as studied by NMR and electronic structure calculations.

50
51
52
53
54
55 (49) Wang, H.; Zhao, E.; Lam, J. W. Y.; Tang, B. Z. *Mater. Today* **2015**, *18*, 365–377. AIE
56 luminogens: emission brightened by aggregation.
57
58
59
60

1
2
3 (50) Pavia, D. L.; Lampman, G. M.; Kriz, G. S. *Introduction to Spectroscopy*; Brooks Cole,
4 Inc. Thomson Learning: Belmont, CA, 2001.
5
6

7
8 (51) Allen, F. H.; Kennard, O.; Watson, D. G.; Brammer, L.; Orpen, A. G.; Taylor, R. *J. Chem.*
9 *Soc., Perkin Trans. 2* **1987**, S1–S19. Tables of bond lengths determined by X-ray and neutron
10 diffraction. Part 1. Bond lengths in organic compounds.
11
12
13
14

15
16 (52) Kitaigorodskii, A. I. *Organic Chemical Crystallography*. Consultant's Bureau: New York,
17 1961. (English translation of the Russian original published by Press of the Academy of Science
18 of the USSR, Moscow, 1955.)
19
20
21
22
23

24 (53) Mercury 3.5.1. <<http://www.ccdc.cam.ac.uk/mercury/>>.
25
26

27 (54) Gavezzotti, A. *Acc. Chem. Res.* **1994**, *27*, 309–314. Are crystal structures predictable?
28
29

30 (55) Gavezzotti, A.; Filippini, G. *J. Phys. Chem. C* **1994**, *98*, 4831–4837. Geometry of the
31 intermolecular X-H.cntdot..cntdot..cntdot.Y (X, Y = N, O) hydrogen bond and the calibration of
32 empirical hydrogen-bond potentials.
33
34
35
36
37

38 (56) Gavezzotti, A. *J. Am. Chem. Soc.* **1983**, *105*, 5220–5225. The calculation of molecular
39 volumes and the use of volume analysis in the investigation of structured media and of solid-
40 state organic reactivity.
41
42
43
44

45 (57) Gavezzotti, A. *Atti Accad. Naz. Lincei, Mem., (Ser. VIII)* **1976**, *13*, 107–119. The 17 two-
46 dimensional space groups: an illustration.
47
48
49

50 (58) Dolomanov, O. V.; Bourhis, L. J.; Gildea, R. J.; Howard, J. A. K.; Puschmann, H. *J. Appl.*
51 *Crystallogr.* **2009**, *42*, 339–341. OLEX2: a complete structure solution, refinement and analysis
52 program.
53
54
55
56
57
58
59
60

1
2
3 (59) Molcanov, K.; Sabljic, I.; Kojic-Prodic, B. *CrystEngComm* **2011**, *13*, 4211–4217. Face-to-
4 face π -stacking in the multicomponent crystals of chloranilic acid, alkali hydrogenchloranilates,
5 and water.
6
7
8

9
10 (60) Gavezzotti, A. *New J. Chem.* **2011**, *35*, 1360–1368. Efficient computer modeling of
11 organic materials. The atom–atom, Coulomb–London–Pauli (AA-CLP) model for intermolecular
12 electrostatic-polarization, dispersion and repulsion energies
13
14
15

16 (61) Gavezzotti, A. *J. Phys. Chem. B* **2003**, *107*, 2344–2353. Calculation of intermolecular
17 interaction energies by direct numerical integration over electron densities. 2. An improved
18 polarization model and the evaluation of dispersion and repulsion energies.
19
20
21
22
23
24

25 (62) Gavezzotti, A. *J. Phys. Chem. B* **2002**, *106*, 4145–4154. Calculation of intermolecular
26 interaction energies by direct numerical integration over electron densities. I. electrostatic and
27 polarization energies in molecular crystals.
28
29
30
31
32

33 (63) Spackman, M. A.; Byrom, P. G. *Chem. Phys. Lett.* **1997**, *267*, 215–220. A novel definition
34 of a molecule in a crystal.
35
36
37
38

39 (64) McKinnon, J. J.; Mitchell, A. S.; Spackman, M. A. *Chem. - Eur. J.* **1998**, *4*, 2136–2141.
40 Hirshfeld surfaces: A new tool for visualising and exploring molecular crystals.
41
42
43
44

45 (65) McKinnon, J. J.; Fabbiani, F. P.; Spackman, M. A. *Cryst. Growth Des.* **2007**, *7*, 755–769.
46 Comparison of polymorphic molecular crystal structures through Hirshfeld surface analysis
47
48
49

50 (66) McKinnon, J. J.; Spackman, M. A.; Mitchell, A. S. *Acta Crystallogr., Sect. B: Struct. Sci.*
51 **2004**, *60*, 627–668. Novel tools for visualizing and exploring intermolecular interactions in
52 molecular crystals.
53
54
55
56
57
58
59
60

1
2
3 (67) Yang, J. S.; Chiou, S. Y.; Liao, K. L. *J. Am. Chem. Soc.* **2002**, *124*, 2518–2527.
4
5 Fluorescence Enhancement of trans-4-Aminostilbene by N-Phenyl Substitutions: The “Amino
6
7 Conjugation Effect”.

8
9
10
11 (68) Cheng, X.; Li, F.; Han, S.; Zhang, Y.; Jiao, C.; Wei, J.; Ye, K.; Wang, Y.; Zhang, H. *Sci.*
12
13 *Rep.* **2015**, *5*, 9140–9147. Emission behaviors of unsymmetrical 1,3-diaryl- β -diketones: A model
14
15 perfectly disclosing the effect of molecular conformation on luminescence of organic solids.

16
17
18
19 (69) Inoue, M.; Hirasawa, I. *J. Cryst. Growth* **2013**, *380*, 169–175. The relationship between
20
21 crystal morphology and XRD peak intensity on $\text{CaSO}_4 \cdot 2\text{H}_2\text{O}$.

22
23
24
25 (70) Anthony, S. P. *ChemPlusChem* **2012**, *77*, 518–531. Organic solid-state fluorescence:
26
27 Strategies for generating switchable and tunable fluorescent materials.

28
29
30 (71) Weissbuch, I.; Torbeev, V. Y.; Leiserowitz, L.; Lahav, M. *Angew. Chem.* **2005**, *117*,
31
32 3290–3293. Solvent effect on crystal polymorphism: Why addition of methanol or ethanol to
33
34 aqueous solutions induces the precipitation of the least stable β form of glycine.

35
36
37
38 (72) Lee, A. Y.; Lee, I. S.; Myerson, A. S. *Chem. Eng. Technol.* **2006**, *29*, 281–285. Factors
39
40 affecting the polymorphic outcome of glycine crystals constrained on patterned substrates.

41
42
43
44 (73) Blagden, N.; J. Davey, R.; F. Lieberman, H.; Williams, L.; Payne, R.; Roberts, R.; Rowe,
45
46 R.; Docherty, R. *J. Chem. Soc., Faraday Trans.* **1998**, *94*, 1035–1044. Crystal chemistry and
47
48 solvent effects in polymorphic systems Sulfathiazole.

49
50
51
52 (74) Heinrich, J.; Ulrich, J. *The 16th International Symposium on Industrial Crystallization*, A-
53
54 13 Dresden, Germany, A-13 Dresden, Germany, 2005; pp 85–90.

1
2
3 (75) Quan, Z.; Wang, Z.; Yang, P.; Lin, J.; Fang, J. *Inorg. Chem.* **2007**, *46*, 1354–1360.

4
5 Synthesis and Characterization of High-Quality ZnS, ZnS:Mn²⁺, and ZnS:Mn²⁺/ZnS (Core/Shell)
6
7
8 Luminescent Nanocrystals.
9

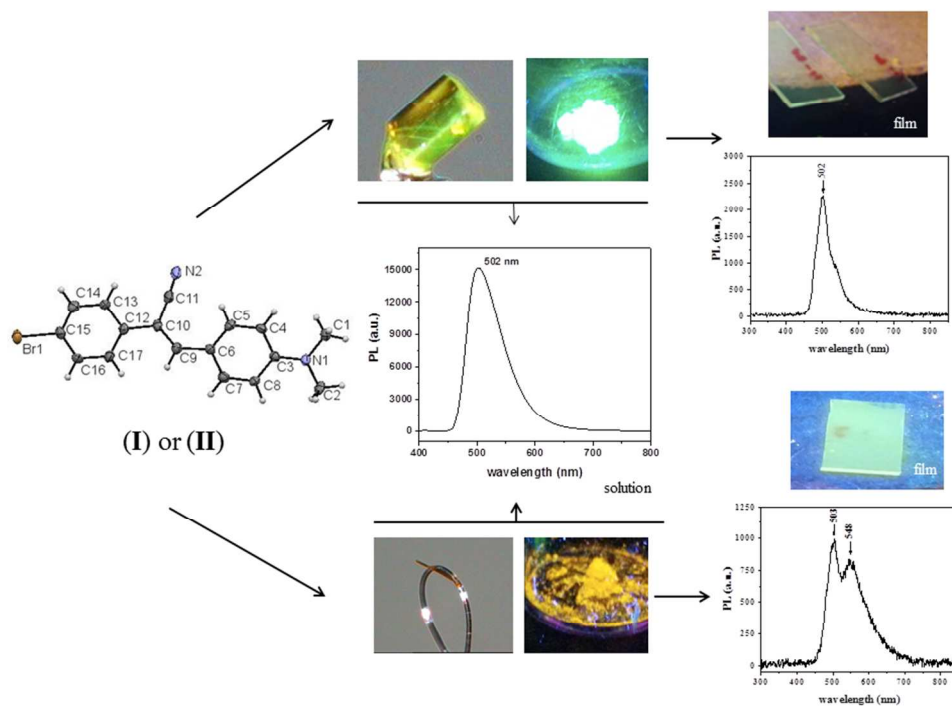
10
11 (76) Pommerehne, J.; Vestweber, H.; Guss, W.; Mahrt, R. F.; Bäessler, H.; Porsch, M.; Daub, J.

12
13 *Adv. Mater.* **1995**, *7*, 551–554. Efficient two layer leds on a polymer blend basis.
14
15
16
17
18
19
20
21
22
23
24
25
26
27
28
29
30
31
32
33
34
35
36
37
38
39
40
41
42
43
44
45
46
47
48
49
50
51
52
53
54
55
56
57
58
59
60

CONSPECTUS GRAPHIC/TABLE OF CONTENTS GRAPHIC

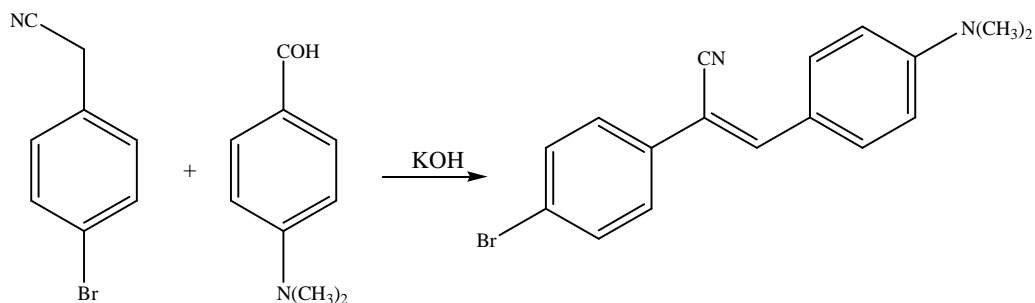
Two different emissions of (2Z)-2-(4-bromophenyl)-3-[4-(dimethylamino)phenyl]prop-2-enitrile due to crystal habit and size: synthesis, optical and supramolecular characterization

Judith Percino,* Margarita Cerón, Perumal Venkatesan, Paulina Ceballos, Alejandro Bañuelos, Oscar Rodríguez, Maxime A. Siegler, Fernando Robles, Víctor M. Chapela, Guillermo Soriano-Moro, Enrique Pérez-Gutiérrez, José Bonilla-Cruz and Subbiah Thamotharan



Crystals of (2Z)-2-(4-bromophenyl)-3-(4-(dimethylamino)phenyl)prop-2-enitrile were yellow blocks (I), and small orange needles (II). The differences between them were the emission wavelength in solid-state due to the morphology, habit and size.

Schemes and Figures



Scheme 1. Reaction to obtain (Z)-2-(4-bromophenyl)-3-(4-[dimethylamino]phenyl)prop-2-enenitrile (Z-4-BrPhDMAPhACN)

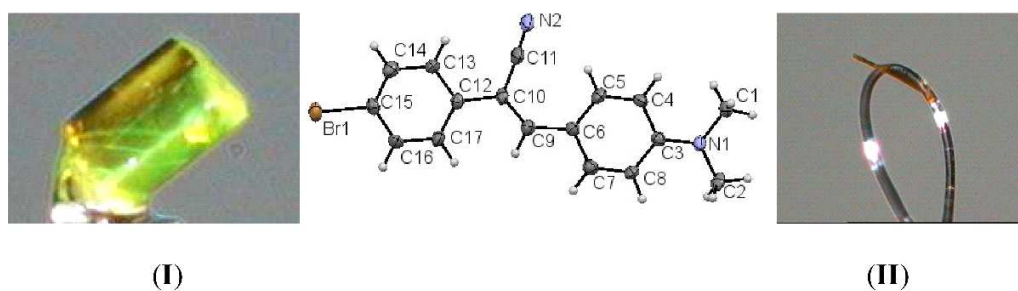


Figure 1. Crystal habits of **I** and **II** and ORTEP diagram of (Z)-2-(4-bromophenyl)-3-[4-(dimethylamino)phenyl]prop-2-enenitrile showing the displacement ellipsoids are drawn at 50% probability level.

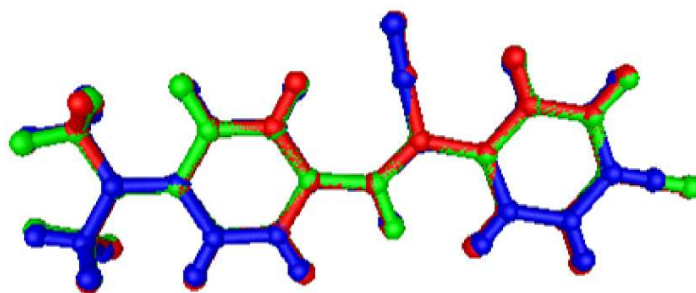
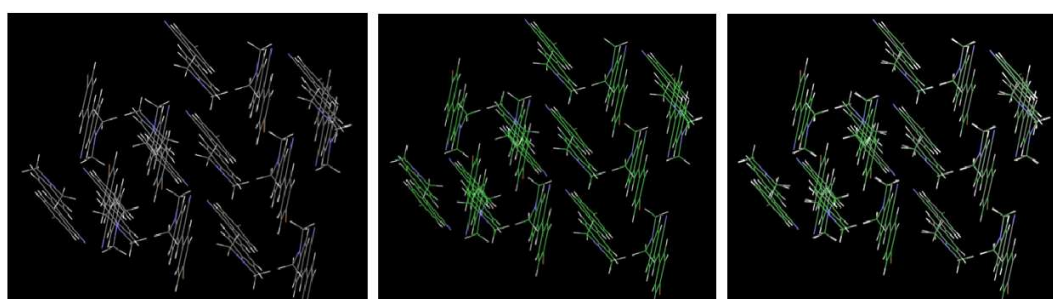
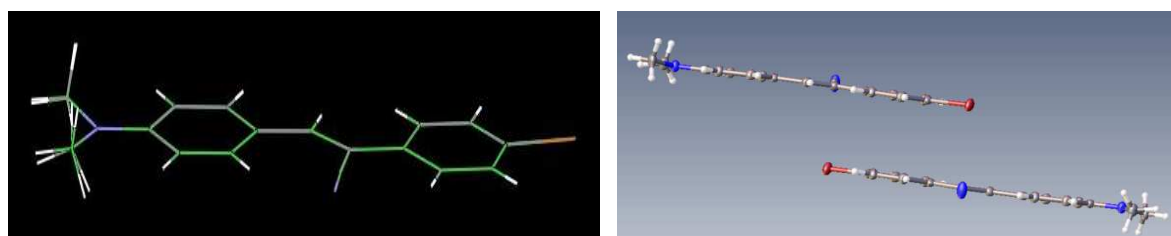


Figure 2. Structural superimposition of **I** (red), **II** (green) and **A** (blue).



(a)



(b)

(c)

Figure 3. Crystal packing diagrams of **I** (gray), **II** (green) and overlap of both (gray-green)⁵³ (a) and molecular structure overlap of **I** and **II** (b), and perspective view of the structures showing the strong $\pi\cdots\pi$ interactions (c).⁵⁸

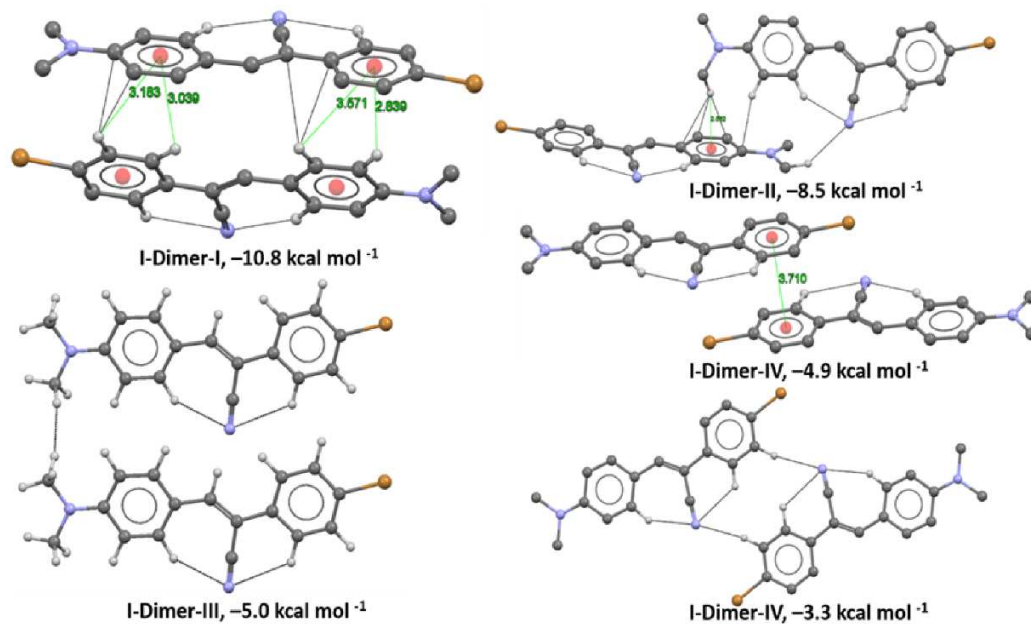


Figure 4. Selected molecular pairs extracted from the crystal structures of **I** and **II** along with their interaction energies (see Table 5).

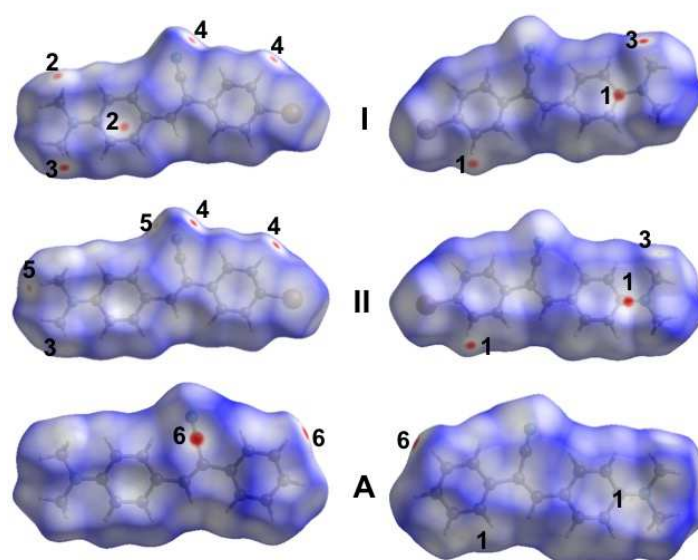


Figure 5. Two different views of the Hirshfeld surfaces mapped with d_{norm} for crystal **I**, crystal **II** and compound **A**. (see Table 5 for the numbering points).

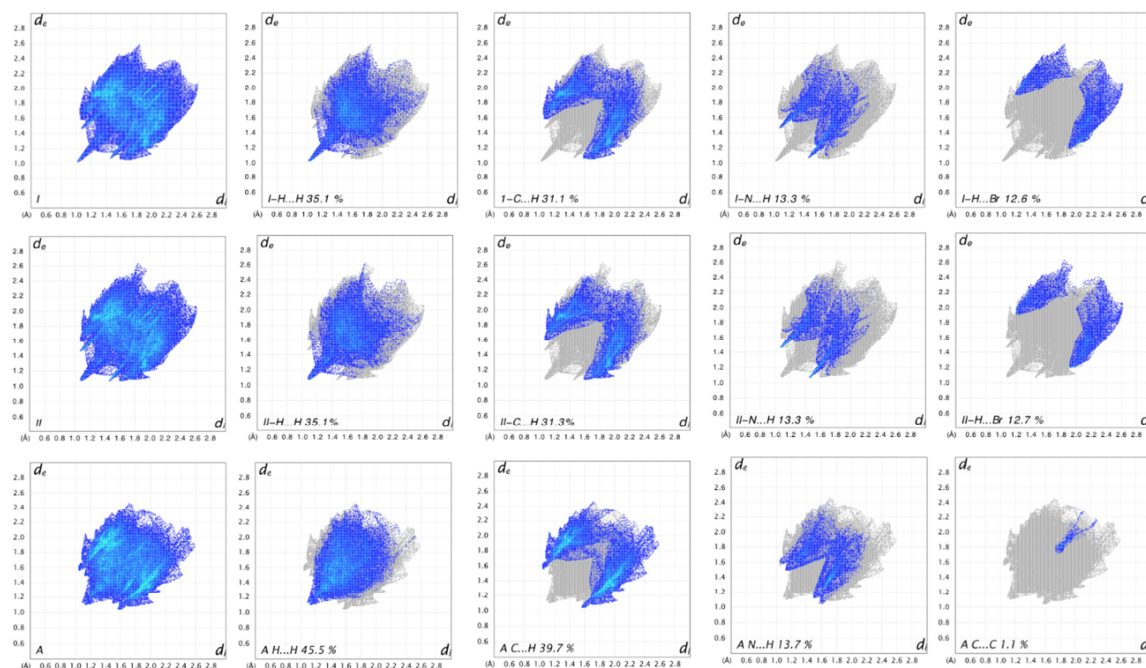


Figure 6. Two-dimensional fingerprint (FP) plots for various intermolecular interactions. The relative of various intermolecular interactions are indicated.

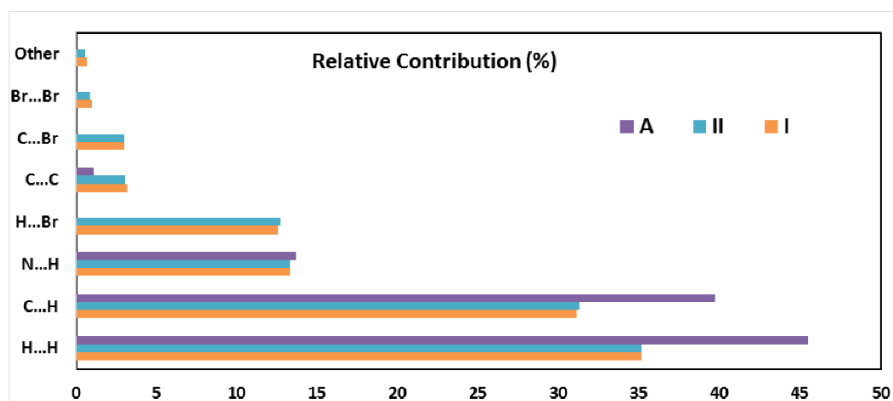


Figure 7. The relative contributions (%) of various intermolecular contacts are present in the structures **I**, **II** and **A**.

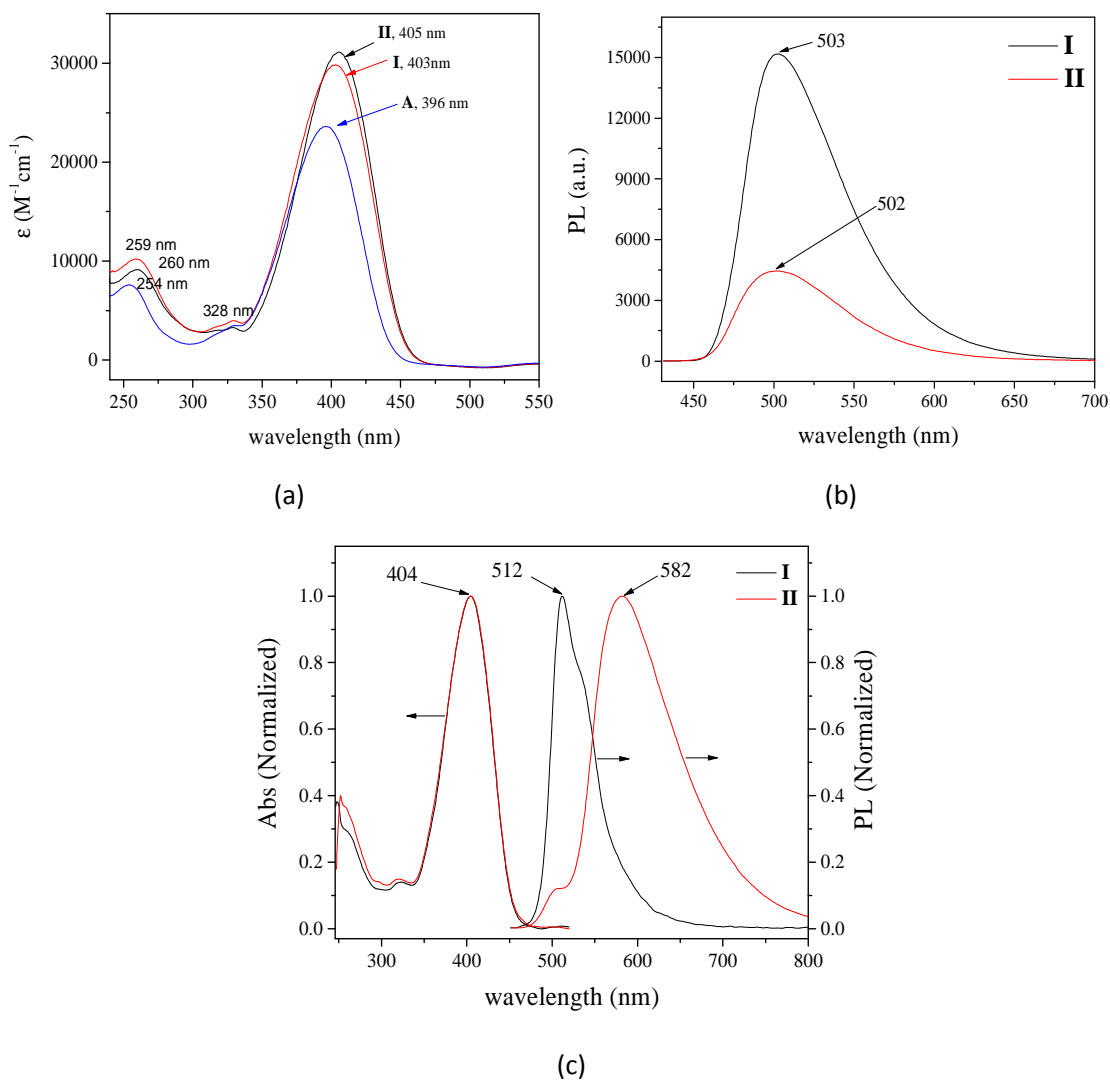


Figure 8. Absorbance spectra of **I**, **II** and **A** in CHCl_3 (a), emission spectra of **I** and **II** in CHCl_3 (b), and the absorption and emission of **I**, **II** in solid state (in KBr) (c).

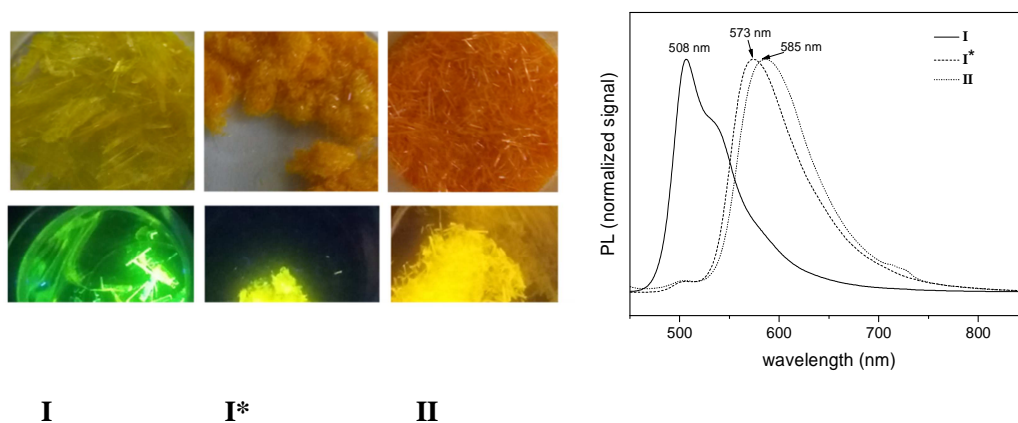


Figure 9. Photographic images showing the crystal habits of **I**, **II**, and the tiny crystals **I***.

The emission spectra of **I**, **II** and **I*** and the PL determined for the three types of crystals.

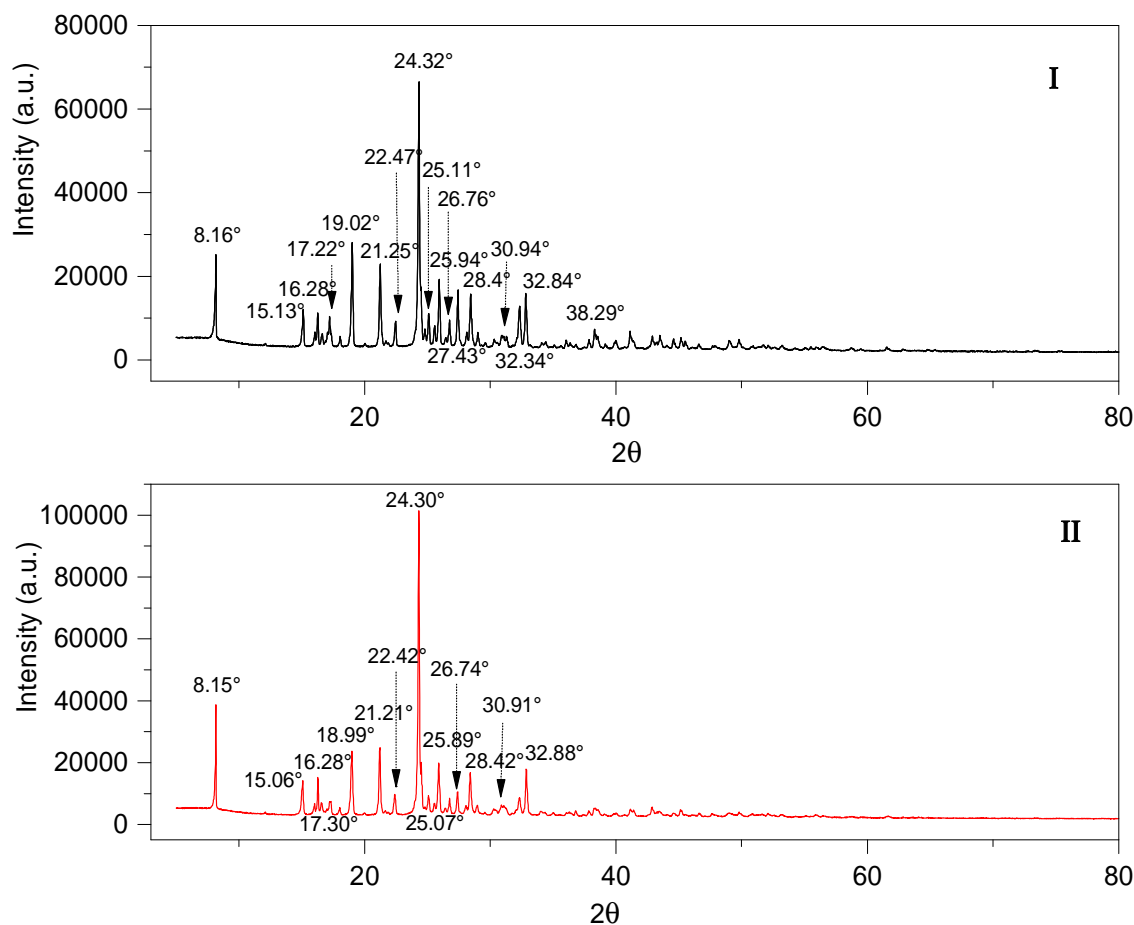


Figure 10. Experimental powder diffraction patterns of **I** and **II**.

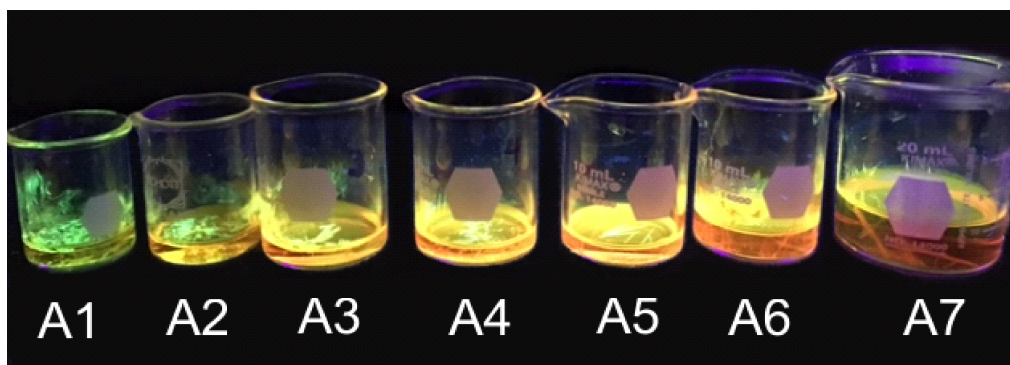
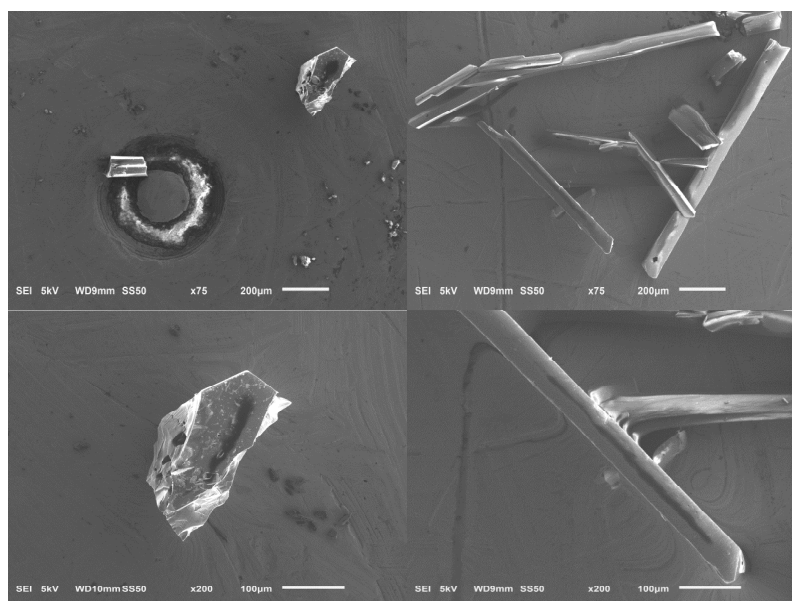
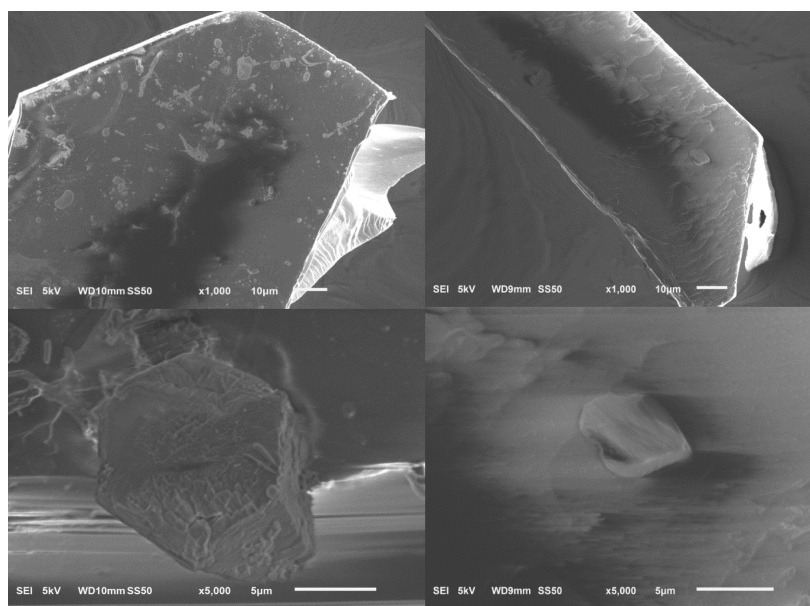


Figure 11. Crystallization of aliquots separated from the solution: A1 (2h), A2 (4h), A3 (6h), A4 (8h), A5 (10h), A6 (12h) and A7 (24h) under UV-vis lamp.

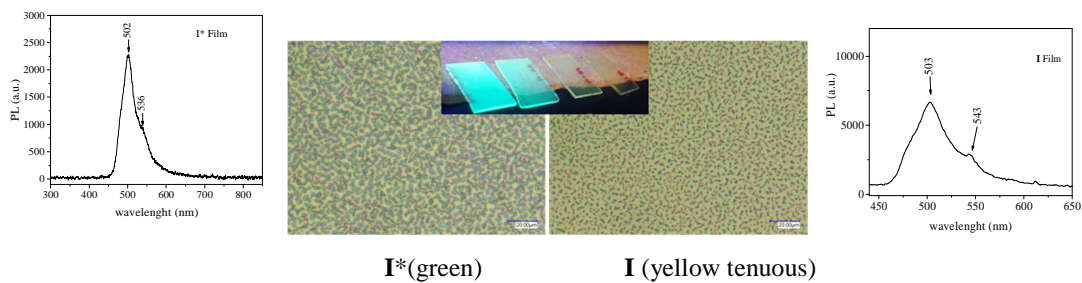


(a)



(b)

26
27
28
29 Figure 12. SEM images of crystals of **I** (a) and **II** (b) at different magnification to look at
30 the effect of different crystallization conditions.
31
32



(a)



(b)

55 Figure 13. Nanocrystals of **I** and **I*** after deposition at high vacuum and their PL spectra of
56 the films under UV source (a) and the PL spectra of the **I*** and **I** in crystal (b).
57
58
59
60

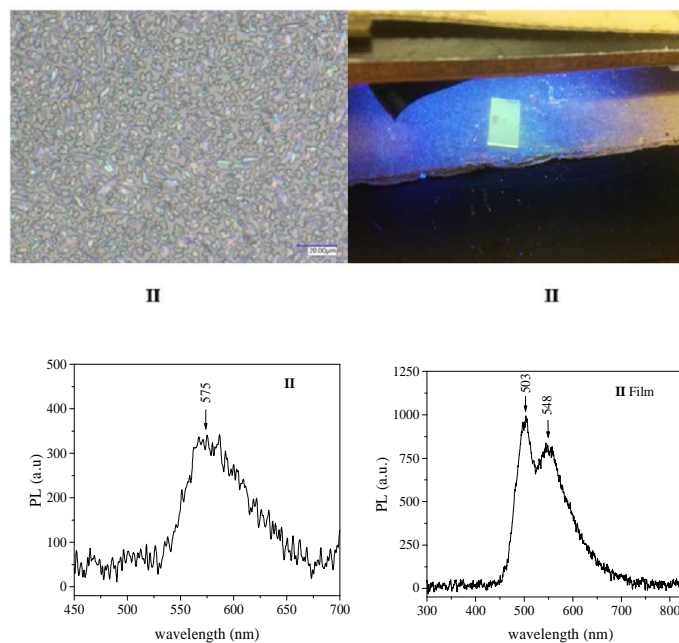


Figure 14. Nanocrystals of **II** deposited by evaporation under high vacuum conditions. Left: PL spectrum of the crystals and right: PL spectrum for the films.

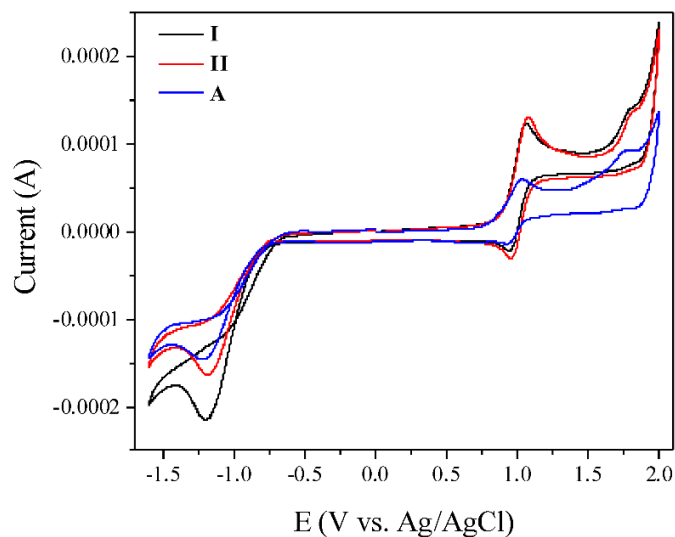


Figure 15. Cyclic voltammograms of **I**, **II** and **A** in 1 mM in 0.1M TBAPF₆/CH₂Cl₂ solution with Ag/AgCl as reference electrode and Pt wire as working electrode. A scan rate of 50 mVs⁻¹ was used.

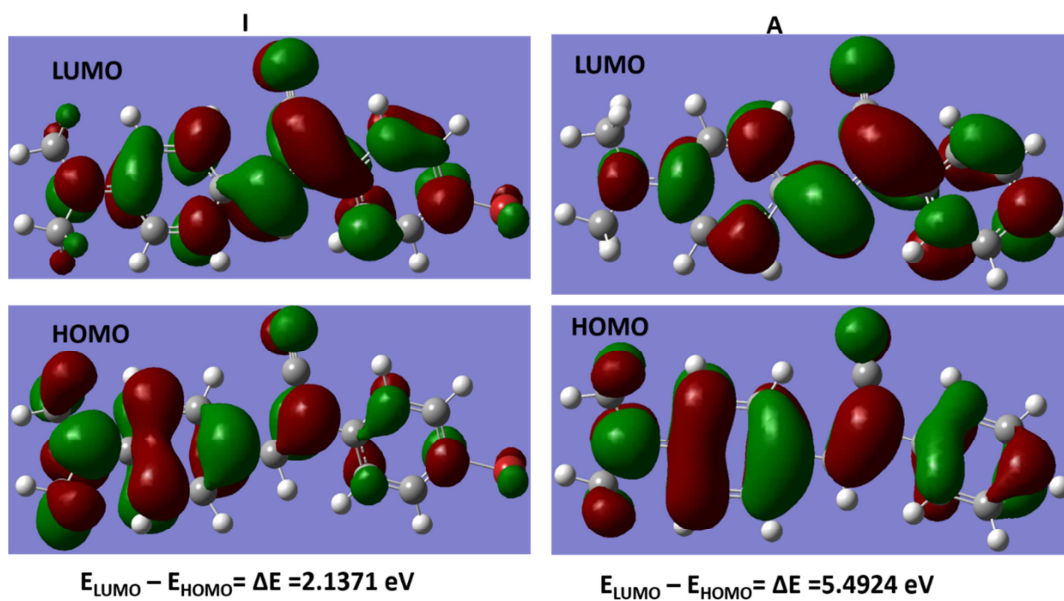


Figure 16. HOMO and LUMO orbitals of **I** and **A**.